Available online at www.sciencedirect.com
SCIENCE DIRECT®
PERGAMON
International Journal of Rock Mechanics & Mining Sciences 40 (2003) 795–816
International Journal of Rock Mechanics and Mining Sciences
www.elsevier.com/locate/ijrmms

Numerical determination of the equivalent elastic compliance tensor for fractured rock masses using the distinct element method

Ki-Bok Min*, Lanru Jing

Department of Land and Water Resources Engineering, Engineering Geology and Geophysics Research Group, Royal Institute of Technology (KTH), S 100 44, Stockholm, Sweden

Accepted 27 February 2003

Abstract

The purpose of this paper is to establish a methodology to determine the equivalent elastic properties of fractured rock masses by explicit representations of stochastic fracture systems, and to investigate the conditions for the application of the equivalent continuum approach for representing mechanical behavior of the fractured rock masses. A series of numerical simulations of mechanical deformation of fractured rock masses at different scales were conducted with a large number of realizations of discrete fracture networks (DFN), based on realistic fracture system information and using the two-dimensional distinct element program, UDEC. General theory of anisotropic elasticity was used for describing the macroscopic mechanical behavior of fractured rock masses as equivalent elastic continua. Verification of the methodology for determining the elastic compliance tensor was conducted against closed-form solutions for regularly fractured rock mass, leading to very good agreements. The main advantage of the developed methodology using the distinct element method is that it can consider complex fracture system geometry and various constitutive relations of fractures and rock matrix, and their interactions. Two criteria for the applicability of equivalent continuum approach were adopted from the investigations: (i) the existence of a properly defined REV (representative elementary volume) and (ii) the existence of an elastic compliance tensor. For the problems with in situ conditions studied in this paper, the results show that a REV can be defined and the elastic properties of the fractured rock mass can be represented approximately by the elastic compliance tensor through numerical simulations.

1. Introduction

1.1. Equivalent continuum approach and discrete approach

Both the equivalent continuum approach and the discrete approach are frequently applied for numerical simulations of mechanical behavior of fractured rock masses. The equivalent continuum approach assumes that macroscopic behavior of fractured rock masses can be described by principles of continuum mechanics, as long as its constitutive relations and associated properties/parameters can be properly established according to the basic laws of continuum mechanics. This is a common modeling approach used in the fields of rock mechanics and hydrogeology, especially for large-scale problems [1,2]. The equivalent continuum approach has the advantage of being more suitable for representing the overall behavior of fractured rock masses for problems of large scales, where the effects of the fractures are implicitly contained in the equivalent constitutive models and associated properties and parameters. The more accurate representations of the local effects of the fractures, especially near the excavations or other sources of man-made or natural disturbances, are sacrificed by representing the averaged overall behavior.

On the other hand, the discrete approach, represented mostly at present by the distinct element method (DEM) and discontinuous deformation analysis (DDA) [3,4], considers that the rocks are assemblies of individual blocks defined by fracture systems, and that the interactions between the rock blocks and fractures (interfaces between blocks) are the main factors affecting the mechanical behavior of the fractured rock masses. Because of the fact that blocks and fracture

*Corresponding author. Tel.: +46-8-790-6807; fax: +46-8-790-6810.
E-mail address: kibok@kth.se (K.-B. Min).

1365-1609/03/$ - see front matter © 2003 Elsevier Ltd. All rights reserved.
doi:10.1016/S1365-1609(03)00038-8

Nomenclature

D fractal dimension for cumulative fracture density characterization

E_x^i, E_y^i, E_z^i elastic moduli of intact rock in x, y and z directions (Pa)

E_x, E_y, E_z elastic moduli in the x, y and z directions (Pa)

EPc_i prediction error of compliance matrix in i direction ($i = x, y$)

G_{yz}, G_{xz}, G_{xy} shear moduli in yz, xz and xy planes (Pa)

$G_{yz}^i, G_{xz}^i, G_{xy}^i$ shear moduli of intact rock in yz, xz and xy planes (Pa)

K_{nx}, K_{ny}, K_{nz} normal stiffnesses of fractures in x, y and z directions (Pa/m)

K_{sx}, K_{sy}, K_{sz} shear stiffnesses of fractures in x, y and z directions (Pa/m)

K ratio of shear stiffness to normal stiffness of fracture

L fracture lengths (m)

N number of fractures greater than a given fracture length per unit area

P fluid pressure (Pa)

Q flowrates of fluids (m^3/s)

q_{ij} contracted direction cosine matrix

S_x, S_y, S_z spacing of fracture sets measured in x, y and z directions (m)

S_{ijkl} elastic compliance tensor by the generalized Hooke's law (1/Pa)

$\bar{S}_{ij}$ average compliance matrix (1/Pa)

s_{ij}^r compliance matrix of the rotated models (1/Pa)

$[\mathbf{S}_{ij}]$ symmetric compliance matrix (1/Pa)

$(S_{ij})^{\mathrm{T}}$ transpose of the compliance matrix (1/Pa)

u_i displacement ($i = x, y, z$)

Greek letters

β_{ij} direction cosines

ε_i normal strain in a contracted form

ε_{ij} strain tensor

γ_{ij} engineering shear strain

$\eta_{x,yz}, \eta_{x,xz}, \eta_{x,xy}, \eta_{y,yz}, \eta_{y,xz}, \eta_{y,xy}, \eta_{z,yz}, \eta_{z,xz}, \eta_{z,xy}$ coefficients of mutual influence of the first kind

$\eta_{yz,x}, \eta_{yz,y}, \eta_{yz,z}, \eta_{xz,x}, \eta_{xz,y}, \eta_{xz,z}, \eta_{xy,x}, \eta_{xy,y}, \eta_{xy,z}$ coefficients of mutual influence of the second kind

φ angle of rotation

μ dynamic viscosity of fluid (Pa · s)

$\mu_{yz,xz}, \mu_{yz,xy}, \mu_{xz,yz}, \mu_{xz,xy}, \mu_{xy,yz}, \mu_{xy,xz}$ coefficients of Chentsov

μ_{EPc} mean prediction error

$\nu_{xy}, \nu_{yx}, \nu_{zx}, \nu_{xz}, \nu_{yz}, \nu_{zy}$ Poisson's ratios

$\nu_{yx}^i, \nu_{zx}^i, \nu_{zy}^i$ Poisson's ratios of intact rock

σ_i normal stress in i direction (Pa)

σ_{kl} stress tensor (Pa)

τ_{ij} shear stress (Pa)

systems are explicitly represented more in detail in the discrete models, the approach is much better equipped to investigate the small-scale, or pseudo-microscopic behavior of a fractured rock mass. This advantage, however, entails sacrificing the problem size since representations of individual blocks and fractures put large demands on computer memory and speed. Therefore, despite the popularity of the 'discrete approach', its applicability to solve practical problems remains to be a challenging task.

Given the fact that many engineering facilities are constructed in fractured rock masses containing extremely large numbers of fractures, it is often necessary to define the behavior of fractured rock masses in 'equivalent' and 'averaged' senses, especially when the sizes of the problems are large and the densities of the fractures are high. Two questions can be raised regarding the application of the equivalent continuum approach.

- The first question is how to determine the mechanical properties of fractured rock masses considering mechanical behavior of both the intact rock and fractures, fracture system geometry and effects of the scales.
- The second is whether the determined mechanical properties are in appropriate forms according to continuum mechanics principles for the description of overall behavior of 'discontinuous' fractured rock masses.

This paper aims to answer the above two questions.

1.2. Methodologies for the determination of the equivalent elastic mechanical properties for fractured rock mass

As for the first question, considerable efforts have been made in the past on the methodology for

determining the equivalent elastic mechanical properties (essentially elastic modulus and Poisson's ratio) of fractured rock mass. Direct measurement by in situ experiments with large or very large-scale samples is technically possible, but is costly and often involves some uncertainties related to the effects of hidden fractures, control of boundary conditions and interpretation of results [5]. Therefore, it is not surprising that significant research efforts have been devoted to indirect ways such as empirical, analytical and numerical methods.

The empirical methods 'infer' the rock mass properties from the rock mass classification or characterization results [1,5–10]. Although it has gained wide popularity for practical applications for design, especially in tunneling, it often gives too conservative estimates for property characterizations, largely because it makes use of categorized parameters based on case histories [11]. The main shortcoming of this approach is that it lacks a proper mathematical platform to establish constitutive models and the associated properties that will not violate the second law of thermodynamics. Furthermore, the anisotropy in the properties cannot be properly represented in tensor form, which is a basic condition of continuum mechanics.

The efforts to find analytical solutions for estimating the equivalent properties of fractured rock masses have a rather long history and several analytical solutions were proposed for cases of simple fracture system geometry [12–18]. The closed-form solutions have the advantage of being compact, clear and straightforward, but they work only for regular, often persistent and orthogonal fracture system geometries and simple constitutive behavior of fractures. It is difficult, often even impossible, to derive closed-form solutions with general irregular fracture systems. The exception in this class of approach is the crack tensor theory that has been applied to find anisotropic elastic properties with irregular fracture systems of different sizes, orientations and fracture properties [19,20]. However, like all analytical methods for fractured rock mass, it does not consider the interaction between the fractures and the blocks divided by the fractures, which may have significant impacts on the overall behavior of rock masses because the intersections of the fractures are often the locations with the largest stress and deformation gradients, damage and failure.

With the rapid growth of computing capacity, numerical methods are attracting more attention to determine individual properties such as strength or deformability of the fractured rock mass [21–22], or to establish systematic methodology of homogenization and upscaling schemes [23–25]. In comparison with the empirical and analytical approaches, the numerical approach has a certain advantage that the influence of irregular fracture system geometry and complex constitutive models of intact rock and fractures can be directly included in the derivation of the equivalent mechanical properties of rock masses. In practice, however, numerical experiments on realistic irregular fracture networks are largely research subjects rather than applicable practicing tools. The main reasons are often the lack of adequate field information regarding fracture system geometry, and the lack of suitable numerical methods and codes for the time-consuming stochastic analyses required.

1.3. Appropriateness of equivalent continuum approach

As to the second question of the appropriateness of continuum mechanics principles, previous studies indicate that great care should be taken [26,27]. Long et al. suggested that two conditions must be satisfied to justify the equivalent continuum approach for fractured rock mass [2].

- Firstly, a representative elementary volume (REV) must exist for a certain problem in order that a basis of statistical equivalence between the sampled rock mass and numerical models can be established and averaging techniques can then be applied over the REV to the derived equivalent properties of homogeneity.
- Secondly, the derived equivalent properties must be represented in tensor form to be used for the constitutive equations for continuum analysis.

In this study, REV is defined as the minimum volume (or a range) beyond which the characteristics of the domain remain basically constant as shown in Fig. 1 [28]. It reflects the scale dependence of the properties of the fractured rock mass due to its fracture population. While investigation of REV has been one of the major subjects in hydraulics of equivalent porous media [29], less work has been devoted to the numerical derivation of the equivalent mechanical properties of fractured rock masses. Controversy also exists for

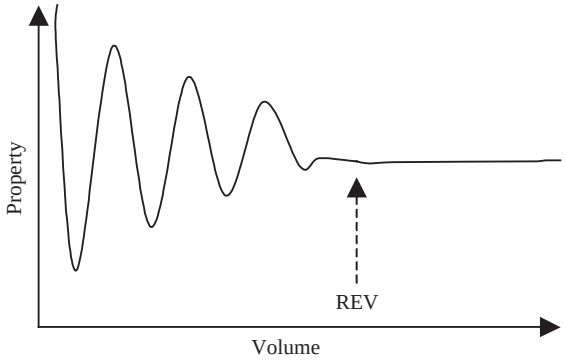

Fig. 1. Representative elementary volume (after [28]).

the justification of the REV concept for fractured rock mass [30].

In addition to the existence of REV, numerical methods based on continuum mechanics principles can be mathematically justified only if the derived elastic properties of rock mass can be represented by a tensor of elastic stiffness or compliance. For problems of fluid flow in fractured rock, it has been suggested that the directional permeability derived should have a tensor quantity for the justification of the continuum approach [2]. We believe that the same is true for the case of mechanical deformation. The only difference between hydraulic and mechanical properties in terms of tensor representation is that compliance tensor in elasticity has a fourth-order rank whereas permeability tensor in hydraulics has a second-order rank. Since the fracture systems often have preferred directions of inclination or strike, tensor representation is needed to include the effects of anisotropy. This cannot be achieved using empirical approaches, and can be achieved by analytical solutions for limited cases of regular and persistent fracture system geometry. For general problems with irregular fracture systems, numerical solution is perhaps the most suitable approach to derive the equivalent properties, their REVs and their representations in tensor form.

1.4. Purpose, methodology and data used in the study

The purpose of this paper is to establish a methodology to determine the equivalent elastic properties of fractured rock masses and to investigate the appropriateness of the equivalent continuum approach for representing the mechanical behavior of the fractured rock mass [31].

In order to represent the fractured rock mass, discrete fracture networks (DFN) were constructed first based on fracture geometry information (orientation, cumulative fracture density and trace lengths) and, on these generated DFN models, numerical experiments were performed using two-dimensional distinct element method program, UDEC [32]. The fractured rock masses are treated as generally anisotropic elastic materials and all the components of compliance tensor in two dimensions are determined through numerical experiments with linearly independent boundary conditions. Intact rock material is assumed to be linear isotropic elastic and the fractures follow an elastic linear model with constant normal and shear stiffness between the contact stresses and displacement for the purpose of simplicity. To verify the applicability of the UDEC approach, an analytical solution for equivalent elastic properties of rock mass intersected by orthogonal fractures is compared with results of the numerical experiments.

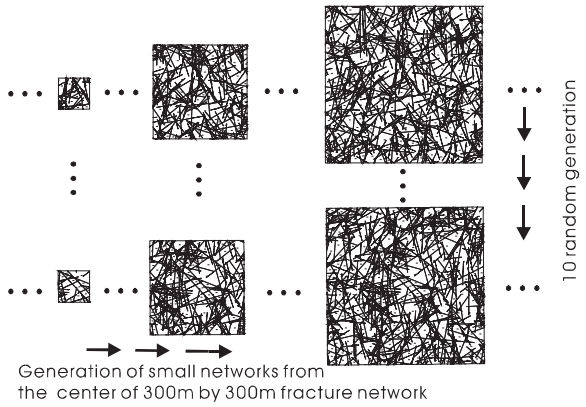

Fig. 2. Schematic view of generations of fracture networks. The size of the square DFN model in the figure is 1 m × 1 m, 3 m × 3 m and 5 m × 5 m, respectively.

The investigation of the appropriateness of equivalent continuum approach was conducted in two ways, corresponding to the two criteria suggested in the previous section. Firstly, to investigate the scale dependency of the fractured rock properties, square computational models of rocks intersected by stochastic fracture systems were generated with sizes varying from 0.25 m × 0.25 m to 8 m × 8 m, with a stepwise increase in size. In order to take into account the stochastic nature of the DFNs based on Monte Carlo simulation, a total of 10 series of DFN models are constructed to investigate the discrepancies created by individual realizations (Fig. 2). To investigate the second criterion, which demands that properties have tensor quantity, one of ten series of models are rotated in clockwise direction with a 30° interval (0°, 30°, 60°, 90°, 120° and 150°) and the same numerical experiments are performed on those rotated models. The calculated mechanical properties are then compared with the predicted values by the tensor transformations. From the investigations using the two criteria, two measures to quantify the variation and errors are suggested for determination of the REV size and equivalent elastic compliance tensor values.

Fig. 3 presents the schematic layout of the motivation and methodologies of this study. The problem is assumed to be two-dimensional and the study is conducted as a part of a Bench-Mark Test in the international DECOVALEX III[1] and BENCHPAR[2] projects with realistic fracture data from site investigations (including orientations, cumulative fracture density, trace lengths of multiple fracture sets) and laboratory experiments of mechanical behavior of intact rocks and fractures, from Sellafield, Cumbria, UK [33].

[1] DECOVALEX III—DEvelopment of Coupled models and their VAlidation against EXperiments in nuclear waste isolation.

[2] BENCHPAR—BENCHmark tests and guidance on coupled processes for Performance Assessment of nuclear waste Repositories.

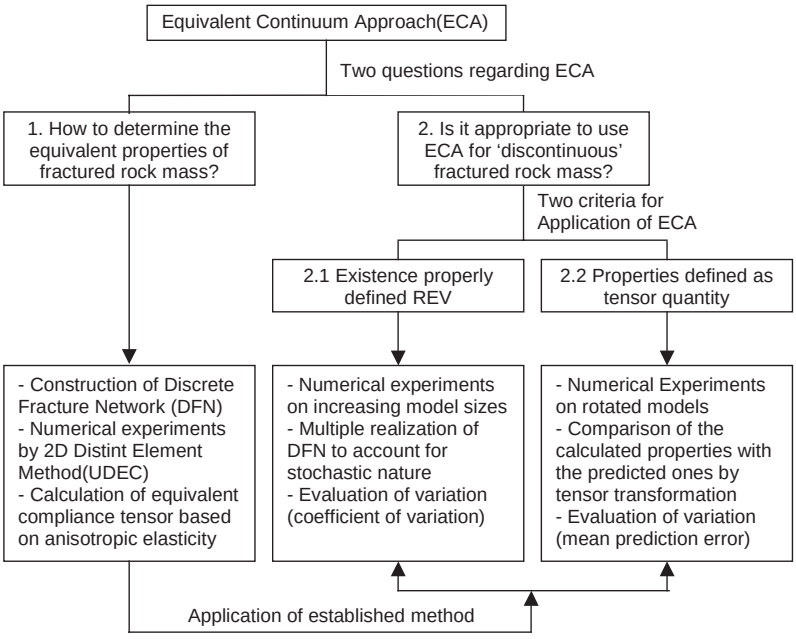

Fig. 3. Motivations and methodologies for this study. Three boxes in the bottom are the methodologies in response to questions and criteria raised. Established method for the calculation of equivalent properties of fractured rock mass (left box of the three boxes in the bottom) are used to investigate the two criteria for the application of equivalent continuum approach (ECA).

2. Some insights into the anisotropic elastic behavior of fractured rock masses

This section briefly presents the general constitutive equation of anisotropic elastic solids and recapitulates some of the important aspects of fractured rock mass behavior from the analytic solutions. It also establishes the foundation of comparison with numerical experiments for verification of the DEM approach proposed in this study.

2.1. Constitutive equation of anisotropic elastic solids and the compliance tensor

The constitutive relation for general linear elasticity can be expressed as [34]

$$\varepsilon_{ij} = S_{ijkl}\sigma_{kl} \tag{1}$$

where ε_{ij} and σ_{kl} are stress and strain tensors of a second order rank and S_{ijkl} is the compliance tensor of a fourth-order rank, involving 21 independent. By adopting a contracted matrix form of S_{ijkl}, Eq. (1) can be expressed as

$$\begin{pmatrix} \varepsilon_x \\ \varepsilon_y \\ \varepsilon_z \\ \gamma_{yz} \\ \gamma_{xz} \\ \gamma_{xy} \end{pmatrix} = \begin{pmatrix} S_{11} & S_{12} & S_{13} & S_{14} & S_{15} & S_{16} \\ S_{21} & S_{22} & S_{23} & S_{24} & S_{25} & S_{26} \\ S_{31} & S_{32} & S_{33} & S_{34} & S_{35} & S_{36} \\ S_{41} & S_{42} & S_{43} & S_{44} & S_{45} & S_{46} \\ S_{51} & S_{52} & S_{53} & S_{54} & S_{55} & S_{56} \\ S_{61} & S_{62} & S_{63} & S_{64} & S_{65} & S_{66} \end{pmatrix} \begin{pmatrix} \sigma_x \\ \sigma_y \\ \sigma_z \\ \tau_{yz} \\ \tau_{xz} \\ \tau_{xy} \end{pmatrix} \tag{2}$$

$$Q_i = A\frac{k_{ij}}{\mu}\frac{\partial p}{\partial x_j} \qquad k'_{ij} = \beta_{im}\beta_{jn}k_{mn}$$

Permeability tensor in generalized darcy's law — 2nd order tensor transformation

$$\varepsilon_{ij} = S_{ijkl}\sigma_{kl} \qquad S'_{ijkl} = \beta_{im}\beta_{jn}\beta_{kp}\beta_{lq}S_{mnpq}$$

Compliance tensor in generalized Hooke's law — 4th order tensor transformation

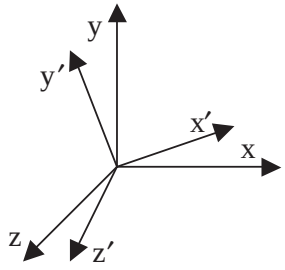

Two coordinate systems for tensor transformations

Fig. 4. Comparison of transformations of permeability and compliance tensor and two coordinate systems.

where matrix S_{ij} is called the compliance matrix. The symbols of ε_i and γ_{ij} $(i,j = x,y,z)$ denote the normal and shear strains, and symbols of σ_i and τ_{ij} $(i,j = x,y,z)$ denote the normal and shear stresses, respectively. The compliance matrix can be described explicitly by giving the physical meaning of each element as functions of elastic moduli, Poisson ratios, shear moduli and other technical constants of the solids [35] (see Appendix A).

Since S_{ijkl} is a fourth-order tensor, its rotational transformation can be also defined by the following mapping operations [34]:

$$S'_{ijkl} = \beta_{im}\beta_{jn}\beta_{kp}\beta_{lp}S_{mnpq} \tag{3}$$

where S'_{ijkl} and S_{mnpq} are the compliance tensors in the transformed and the original axes, respectively, and β_{im} is direction cosines representing rotational operations. Fig. 4 shows the comparison between a second-order permeability transformation and a fourth-order compliance tensor transformation. Eq. (3) is mathematically elegant but not convenient for practical calculations because it involves fourth order tensor operations. The following mapping operation with a 6×6 matrix for the transformation of compliance matrix is introduced to simplify the operations [35]:

$$S'_{ij} = S_{mn}q_{mi}q_{nj} \tag{4}$$

where S'_{ij} is the compliance matrix in the transformed axes and S_{mn} is the one in the original axes, respectively. The component of the q_{ij} matrix is described in Appendix B. When only the rotation of axes is concerned, the transformation form becomes drastically simple. If the angle of anti-clock wise rotation of axes about z axis is φ, the matrix of the direction cosines is then given by

$$\beta_{ij} = \begin{pmatrix} \cos\varphi & \sin\varphi & 0 \\ -\sin\varphi & \cos\varphi & 0 \\ 0 & 0 & 1 \end{pmatrix} \tag{5}$$

and the final matrix form for q_{ij} has the following form:

$$q_{ij} = \begin{pmatrix} \cos^2\varphi & \sin^2\varphi & 0 & 0 & 0 & -2\sin\varphi\cos\varphi \\ \sin^2\varphi & \cos^2\varphi & 0 & 0 & 0 & 2\sin\varphi\cos\varphi \\ 0 & 0 & 1 & 0 & 0 & 0 \\ 0 & 0 & 0 & \cos\varphi & \sin\varphi & 0 \\ 0 & 0 & 0 & -\sin\varphi & \cos\varphi & 0 \\ \sin\varphi\cos\varphi & -\sin\varphi\cos\varphi & 0 & 0 & 0 & \cos^2\varphi - \sin^2\varphi \end{pmatrix} = Q \tag{6}$$

Therefore, by inserting the matrix of Eq. (6) into Eq. (4), it is possible to express the elastic constants, i.e. elastic modulus or Poisson's ratio, in rotated axes in terms of direction cosines and components in the original axes. The above rotational mapping relations are important for comparing elastic compliance tensors derived for different DFN models in the latter part of this paper.

2.2. Closed-form solutions for fractured rock masses with persistent orthogonal sets of fractures

The compliance tensor of a rock mass with three sets of orthogonal persistent fractures in three-dimension is constructed by superimposing the fracture constitutive relation on the compliance matrix of intact rock, by treating the rock mass as an orthotropic elastic material [17], given by

$$\begin{pmatrix} \frac{1}{E^i_x}+\frac{1}{K_{nx}S_x} & -\frac{\nu^i_{yx}}{E^i_y} & -\frac{\nu^i_{zx}}{E^i_z} & 0 & 0 & 0 \\ -\frac{\nu^i_{yx}}{E^i_y} & \frac{1}{E^i_y}+\frac{1}{K_{ny}S_y} & -\frac{\nu^i_{zy}}{E^i_z} & 0 & 0 & 0 \\ -\frac{\nu^i_{zx}}{E^i_z} & -\frac{\nu^i_{zy}}{E^i_z} & \frac{1}{E^i_z}+\frac{1}{K_{nz}S_z} & 0 & 0 & 0 \\ 0 & 0 & 0 & \frac{1}{G^i_{yz}}+\frac{1}{K_{sy}S_y}+\frac{1}{K_{sz}S_z} & 0 & 0 \\ 0 & 0 & 0 & 0 & \frac{1}{G^i_{xz}}+\frac{1}{K_{sx}S_x}+\frac{1}{K_{sz}S_z} & 0 \\ 0 & 0 & 0 & 0 & 0 & \frac{1}{G^i_{xy}}+\frac{1}{K_{sx}S_x}+\frac{1}{K_{sy}S_y} \end{pmatrix} \tag{7}$$

where E^i_x, E^i_y, E^i_z are the elastic moduli of the intact rock matrix in x, y and z directions, G^i_{yz}, G^i_{xz}, G^i_{xy} are the shear moduli of the intact rock matrix in yz, xz and xy

planes, and v_{yx}, v_{zx}, v_{zy} are the Poisson ratios of the intact rock matrix, respectively. The symbol v_{ij} is Poisson's ratio of normal strain in the j direction to that in the i direction when stress is applied in the i direction. K_{nx}, K_{ny}, K_{nz} are the normal stiffness of fractures in x, y and z directions,K_{sx}, K_{sy}, K_{sz} are the shear stiffness of fractures in x, y and z directions, and S_x, S_y, S_z are the spacing of fracture sets measured in x, y and z directions, respectively (Fig. 5). The compliance matrix in Eq. (7) can also be expressed in the transformed axes using Eq. (4).

As an example of the application of compliance matrix rotation by Eqs. (4) and (7) in a two dimensional case, Fig. 6 presents the variation of elastic moduli according to the rotation of axis with two orthogonal sets of fractures. This type of polar diagram was first presented by Wei [36,37] based on the crack tensor theory with infinitely persistent fractures, demonstrating the variation of elastic modulus in various fracture conditions including geometry, stiffness and dilation. To investigate the effects of fracture properties on the overall behavior of the fractured rock mass, variation in the elastic moduli is plotted according to different K ratios, which is defined as the ratio of shear stiffness to normal stiffness of fractures. Two hypothetical cases are considered and Table 1 shows the properties used for the solutions. Case 1 is when the normal stiffness of both fracture sets are the same and Case 2 is when the normal stiffness of fracture set 2 (horizontal fractures) is 50% of that of set 1 (vertical fractures). Both cases give us a good insight into the anisotropic behavior of fractured rock masses and the following points are worth noting.

Firstly, when $K = 1.0$, the fractured rock mass shows complete isotropic behavior with identical normal stiffness for both fracture sets (Case 1). However, even when K equals 1.0, anisotropy appears if the normal stiffnesses of fracture sets are different (Case 2).

Secondly, when K is smaller than 1.0, anisotropic behavior becomes significant and this case has more relevant implications since K value of a realistic rock mass is usually far less than 1.0. For instance, when K equals 0.1 in Case 1, which may be close to the case of a realistic rock mass, the smallest elastic modulus is observed in the 45° direction and its value is only 8%

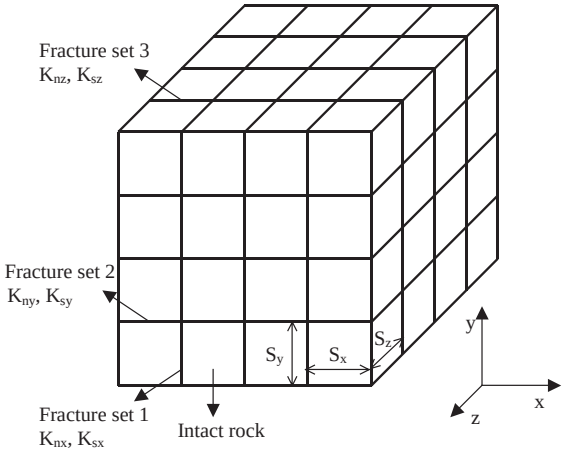

Fig. 5. Simplified diagram for the reference axes and rock blocks. Explanations of parameters are given in the text.

Table 1
Parameters used for calculation of variation of modulus

Properties	Case 1	Case 2
Elastic modulus (GPa)	50	50
Poisson's ratio	0.25	0.25
Fracture normal stiffness (GPa/m)	50 (set 1 = set 2)	50 (set 1) 25 (set 2)
Fracture shear stiffness (GPa/m)	5–250	5–250 (set 1) 2.5–125 (set 2)
Spacing of fracture sets (m)	0.5	0.5

Set 1 is vertical and Set 2 is horizontal set.

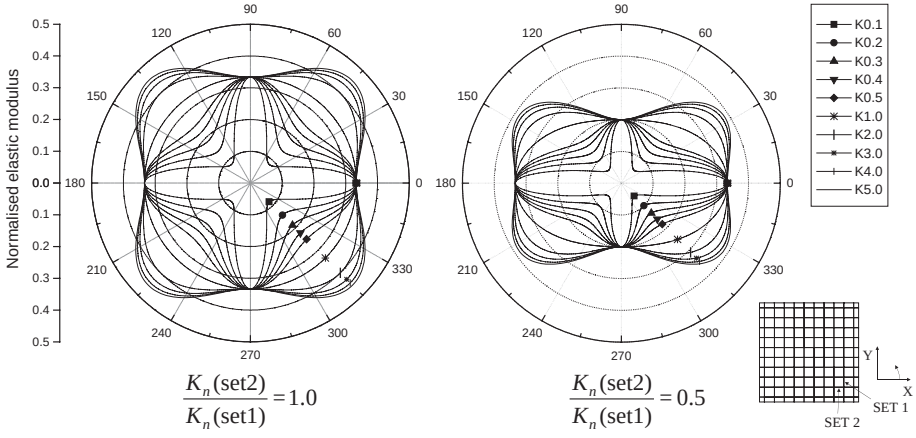

Fig. 6. Variation of elastic modulus of fractured rock mass with two orthogonal sets of fractures according to different K ratios (shear to normal stiffness ratio). Two cases when normal stiffness of two sets are the same and normal stiffness of set 2 is half of that of set 1 are presented (reconstructed from [37]).

of intact rock modulus, whereas the ratio for the maximum elastic modulus is 33%. For Case 1, the direction of minimum modulus is 45° but in Case 2, it approaches 45° with a decreasing K ratio.

Thirdly, when K is larger than 1.0, the maximum modulus is observed between two fracture planes in both cases. However, this may only be possible for reinforced fractures (e.g. by grouting or bolting) where the shear stiffness could be larger than normal stiffness.

As was seen here, the behavior of a fractured rock mass is significantly different from that of isotropic intact rock due to the presence of fractures. Hence, it points out the need to consider the anisotropy issue when deriving the rock mass properties.

The closed-form solution introduced here also provides a verification basis for applicability of the DEM approach as described in Section 4 of this paper.

3. Stochastic discrete fracture network (DFN) analysis

An independent stochastic DFN generation program is developed for the generations of realistic DFN models. The methodology for the program is largely based on the approach suggested in [38,39] with extensions to consider boundary effects and the fractal relations between the fracture density and trace length. The generated fracture networks are used as geometrical models for the UDEC simulations. This section briefly explains the approach of generating DFN realizations, and more detailed explanation can be found in [31,40].

3.1. Data of fractures used for the analysis

From the site investigation, four sets of fractures are identified and the orientations of fracture sets are shown to follow Fisher distributions. The data set shows highly fractured rock condition with high fracture densities and the highly dispersed patterns with low Fisher constants. Table 2 shows the basic information about the fracture systems and properties of intact rock and fractures. The normal stiffness of fractures was taken as the mean value of the normal stiffness of four samples, determined from the fourth-cycle of displacement–load curve to consider the disturbance during the specimen acquisition. The shear stiffness values were assumed to be 20% and 100% of normal stiffness for sensitivity studies. These mechanical properties of fractures are assigned to all four fracture sets. The fracture trace lengths are characterized by a fractal scaling law as given in [41]:

$$N = 4 \times L^{-D} \tag{8}$$

where D is the fractal dimension and N is the number of fractures greater than a given fracture length L (m) per unit area (m^2). Fractal dimension (D) from the site characterization was 2.2 ± 0.2, and the value 2.2 is used for this study. The minimum and maximum cutoff trace lengths are chosen as 0.5 and 250 m, respectively.

3.2. Stochastic discrete fracture network generation

The Monte Carlo simulation approach is used to generate the DFN models, based on distribution functions of location, orientation, trace-length and density of fractures. A Poisson's process is applied to generate the locations of the fracture centers, as are conventionally used in similar practice. Fracture trace lengths are generated with the cumulative probability density function of trace length, which can be determined from the given cumulative density of fractures with minimum and maximum cutoff lengths. The orientations of the fractures are generated by using the Fisher distributions of fracture sets, which involves the generation of the deviation angle from the mean orientation angle of the set based on a probability density function, followed by converting the orientation data from three to two dimensions.

A boundary effect can be caused by the fact that the centers of some large fractures may not necessarily lie

Table 2
Parameters for DFN analysis

Intact rock		Fractures						
Elastic modulus (GPa)	Poisson's ratio	Set	Dip/Dip direction	Fisher constant (K)	Normal stiffness (GPa/m)	Shear stiffness (GPa/m)	Fracture density[a] (m^{-2})	Mean trace length[b] (m)
84.6	0.24	1	8/145	5.9	434	86.8/434	4.6	0.92
		2	88/148	9.0	434	86.8/434	4.6	0.92
		3	76/21	10.0	434	86.8/434	4.6	0.92
		4	69/87	10.0	434	86.8/434	4.6	0.92

[a] Fracture density is calculated from the cumulative number of fractures with minimum and maximum cutoff trace lengths by Eq. (8).
[b] Mean trace length is measured from the generated fracture network with the minimum and maximum cutoff trace lengths.

inside the domain of computational models and this can result in the underestimation of effects of larger fractures intersecting the computational domain. To avoid this boundary effect, the parent DFN models should be at least larger than the maximum cutoff length of fractures [40]. In this study, test models are cut from sufficiently large parent DFN models of 300 m × 300 m in size to account for effects of the maximum trace length of 250 m.

3.3. Procedure of DFN generation

To properly represent the stochastic nature of DFN generation, ten series of DFN models are generated to ensure that the calculated results are not dependent on one single numerical experiment and to produce more representative stochastic behavior of the fractured rock mass. From each generated parent network, increasingly large models are cut out from the center of the parent models, in sizes from 0.25 m × 0.25 m to 8 m × 8 m scale. The small size of 0.25 m and 0.5 m are chosen to see the effect of the minimum cutoff length of 0.5 m. To investigate the tensor quantity of the models, one of the series are rotated in clockwise direction with a 30° interval (0°, 30°, 60°, 90°, 120°, 150°). Table 3 presents the complete lists of generated models and numerical experiments for scale dependency and tensor quantity evaluation.

Fig. 7 shows examples of generated fractures with ten realizations (DFN1–DFN10) at the 5 m × 5 m scale. It should be noted that all models have slightly different patterns depending on the individual Monte Carlo simulation even though they have the same fracture statistics.

Table 3
Complete lists of generated model and numerical experiments

Geometry	Side length of model (m)										Comments
	0.25	0.5	1	2	3	4	5	6	7	8	
DFN1	●	●	●	●	●	●	●	●	●	●	
DFN2	●	●	●	●	●	●	●	●	●	●	
DFN3	●	●	●	●	●	●	●	●	●	●	
DFN4	●	●	●	●	●	●	●	●	●	●	
DFN5	●	●	●	●	●	●	●	●	●	●	
DFN6	●	●	●	●	●	●	●	●	●	●	
DFN7	●	●	●	●	●	●	●	●	●	●	
DFN8	●	●	●	●	●	●	●	●	●	●	
DFN9	●	●	●	●	●	●	●	●	●	●	
DFN10	●	●	●	●	●	●	●	●	●	●	
DFN1_30	●	●	●	●	●	●	●	●	●	—	Models are rotated at 30°,60°,90°,120°,150° from DFN1
DFN1_60	●	●	●	●	●	●	●	●	●	—	
DFN1_90	●	●	●	●	●	●	●	●	●	—	
DFN1_120	●	●	●	●	●	●	●	●	●	—	
DFN1_150	●	●	●	●	●	●	●	●	●	—	

Marks (●) indicate that models are generated and numerical experiments are performed.

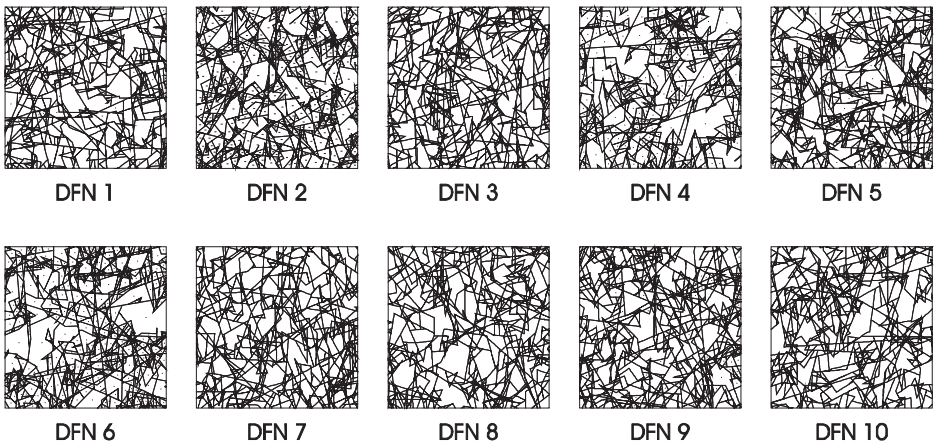

Fig. 7. Discrete fracture network models with 10 realizations(5 m × 5 m scales are shown here as examples). DFN1, DFN2,…,DFN10 denotes the different random realization.

4. Modeling approach using the UDEC code

4.1. Methodology for the determination of the compliance matrix

Since the shear strain and shear stress components associated with z direction can be removed for two-dimensional plane strain analyses, Eq. (2) can be reduced to the following form:

$$\begin{pmatrix} \varepsilon_x \\ \varepsilon_y \\ \varepsilon_z \\ \gamma_{xy} \end{pmatrix} = \begin{pmatrix} S_{11} & S_{12} & S_{13} & S_{16} \\ S_{21} & S_{22} & S_{23} & S_{26} \\ S_{31} & S_{32} & S_{33} & S_{36} \\ S_{61} & S_{62} & S_{63} & S_{66} \end{pmatrix} \begin{pmatrix} \sigma_x \\ \sigma_y \\ \sigma_z \\ \tau_{xy} \end{pmatrix} \tag{9}$$

The components related to normal stress in z direction need to remain since generated σ_z due to the confinement of z direction displacement affects the deformation in x and y directions. Considering the fact that there is no effect of out-of-plane fractures (which means that the fractures in the UDEC model conceptually have the strike in the direction of out-of-plane, z direction) the elastic modulus in z direction (E_z) can be predetermined as the elastic modulus of intact rock. Furthermore, if we consider the symmetry conditions, $S_{13} = S_{31}$, $S_{23} = S_{32}$ and $S_{36} = S_{63}$, which are associated with z directional stress and strains, eventually only three components are independent in each row of the matrix. Therefore, three linearly independent stress boundary conditions are sufficient to determine all components in the matrix shown in Eq. (9).

In fact, all the components related to σ_z can be predetermined. As shown in Fig. 8, the values of elements S_{13} and S_{23} can be determined considering that the v_{zx} and v_{zy} are the same as Poisson's ratio of intact rock. Furthermore, S_{36} will be zero since shear stress τ_{xy} does not affect the z directional deformation.

4.2. Numerical experiments by DEM modeling and verification

The generated DFN models are discretized with triangular zones of constant strains for distinct element analysis using the UDEC code, with the linear size of triangular zones varying from 0.002 to 0.1 m (Fig. 9). The maximum number of internal zones to be analyzed for this study is about 50,000 with 5000 blocks at the 8 m × 8 m scale.

Fig. 10 illustrates the three linearly independent boundary conditions (BC1–BC3) used to produce the two-dimensional compliance matrix in Eq. (9). BC1 consists of biaxial normal stresses and BC2 is created by sequentially increasing the normal stress in the y direction. Even though one additional normal stress increment in the y direction suffices for the purpose of BC2, two to four sequential y directional normal stress

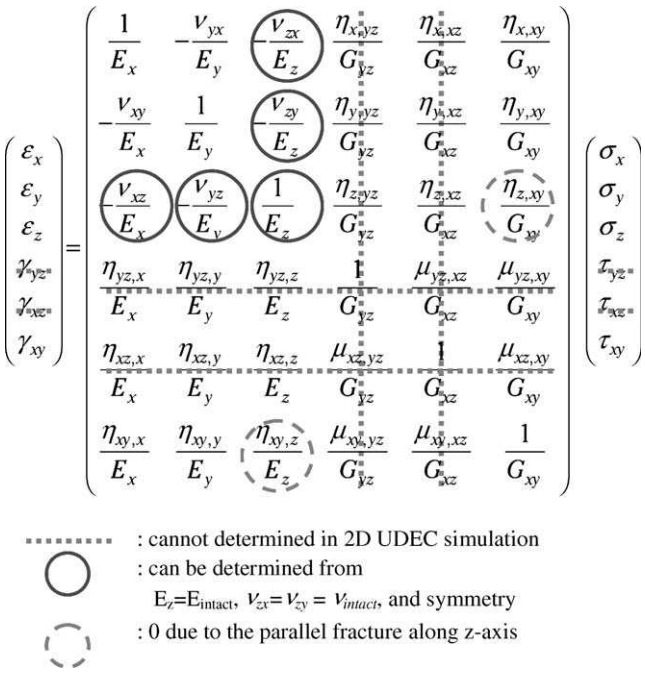

Fig. 8. Conceptualization for the determination of compliance matrix.

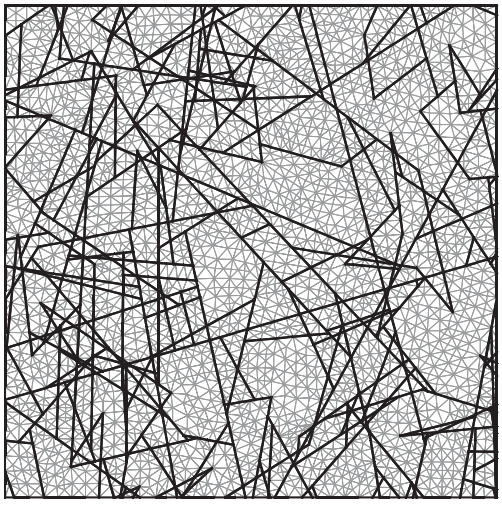

Fig. 9. Examples of discretized DFN model (3 m × 3 m model, DFN3, 612 blocks and 6234 internal zones).

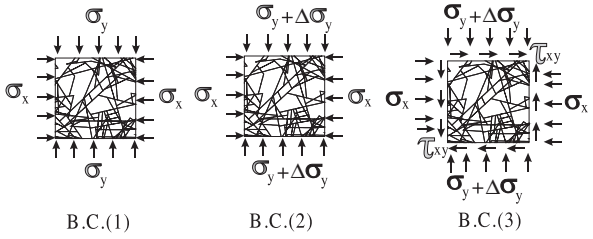

Fig. 10. Three linearly independent boundary conditions for numerical experiments.

increments were applied to check the linearity of the mechanical behavior. Similarly, BC3 is created by sequentially superimposing shear stress increments over the stress conditions of the final BC2. Three to five sequential shear stress increments were applied to see the linearity of the model response. If the linearity is observed, the final stress and strain states of the DFN models for each boundary condition were used for calculation of compliance tensor.

For calculation of the average strain values in the domain, eleven parallel sampling lines within each model are set in both x and y directions, with the same distance in between. Strain components are then calculated from displacement values according to the following strain–displacement relationship:

$$\varepsilon_{ij} = \tfrac{1}{2}(u_{i,j} + u_{j,i}) \tag{10}$$

where u_i $(i = x, y)$ is the displacement components along the sampling lines.

In order to verify the methodology proposed above, a model with two orthogonal fracture sets is used for the comparison between the elastic properties produced by the numerical experiments and the close-form solutions using Eqs. (4) and (7). The computational models are rotated in intervals of 10° to evaluate the variation of elastic moduli in rotated directions (Fig. 11). Note also that the model boundary is located in the center of fracture spacing to avoid the need to adjust the equivalent spacing [32]. Table 4 lists the parameters used for this verification. Three boundary conditions described in Fig. 10 are applied to obtain the compliance matrix. Since the model is symmetric about x and y axis when properties of two fracture sets are the same, only values from 0° to 90° are compared. As shown in Fig. 12, the two sets of results show an almost perfect agreement. Therefore, it is reasonable to conclude that the methodology adopted for numerical approach using the UDEC code can be used for more complex cases of irregular fracture system geometry.

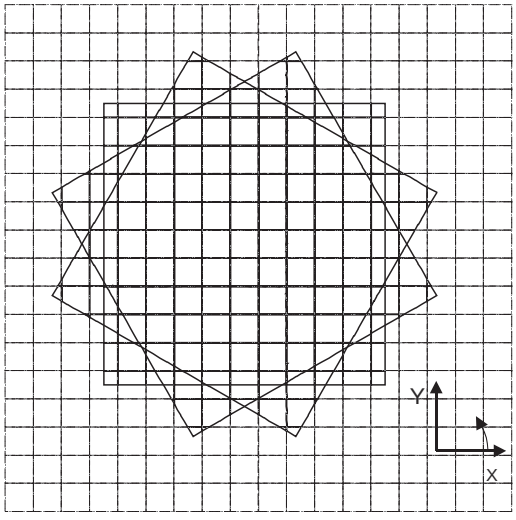

Fig. 11. Rotated computational models with two perpendicular sets of persistent fractures. The models in the figures are examples of 0°, 30° and 60° rotations.

Table 4
Parameters used for the verification of UDEC modeling

Properties	
Elastic modulus (GPa)	84.6
Poisson's ratio	0.24
Fracture normal stiffness (GPa/m)	434
Fracture shear stiffness(GPa/m)	43.4–2170
Spacing of fracture sets (m)	0.5

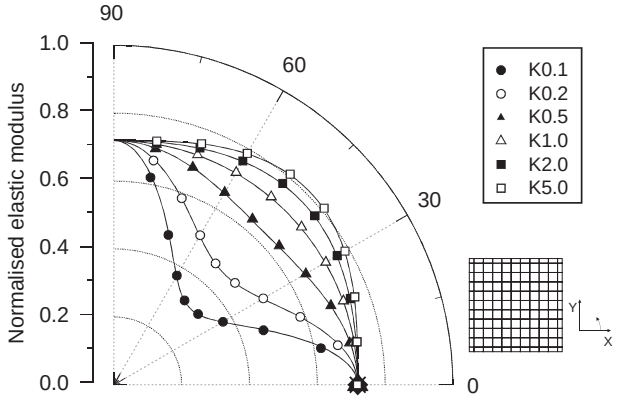

Fig. 12. Verification of UDEC modeling results against analytical solution for a fractured rock mass with two orthogonal sets of fractures. Points of symbols correspond to numerical results with different K ratio values and the lines are the analytical solutions.

4.3. Deformation characteristics during the numerical experiments by DEM modeling

Fig. 13 shows the contours of the y directional displacement of the fractured rock mass under biaxial loading (BC2) from one of the UDEC models for the purpose of a demonstration. Note that zero displacement lies in the center of the model since stresses were applied on both sides. It shows that although the displacement distribution is much influenced by the deformation of fractures, a general trend of roughly uniform deformation gradient can still be observed due to the collective contributions of large numbers of fractures. Averaging process is therefore applicable to derive mean values of displacements gradients and strains. Dead-ends of fractures are not incorporated in existing UDEC code and its effect is assumed not to be significant.

Fig. 14 presents the stress–strain relationship obtained with two boundary conditions, BC1 and BC2 for model DFN3 at 3 m × 3 m scale. After applying the

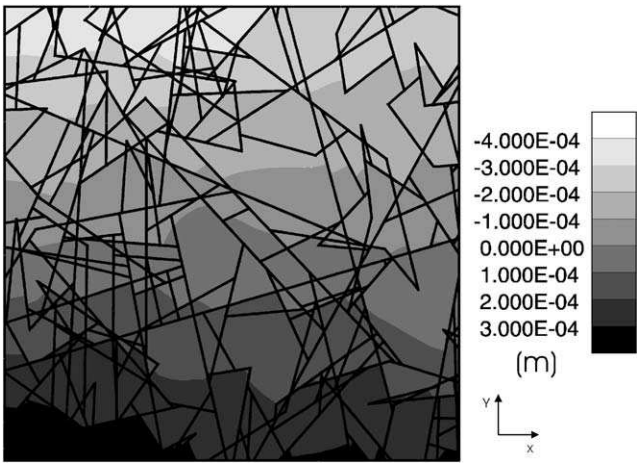

Fig. 13. The Y displacement contours under biaxial compressive loading ($\sigma_x = -5$ MPa, $\sigma_y = -10$ MPa, size 3 m × 3 m, DFN 3).

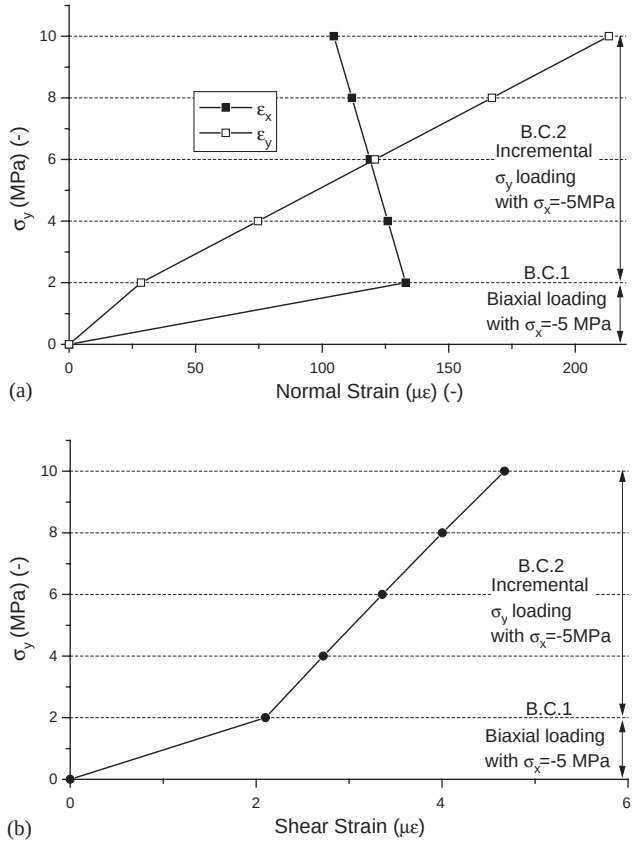

Fig. 14. Stress–strain relation from the sequential numerical experiment (normal stress loading stage, BC1 and BC2). Model is from DFN3 with size 3 m × 3 m. (a) normal stress-normal strain relationship and (b) normal stress–shear strain relationship. Compressive normal is denoted (−) and shear stress acting in the positive direction in positive face of element is (+).

BC1 boundary condition of $\sigma_x = -5$ MPa and $\sigma_y = -2$ MPa, σ_y is then sequentially increased from −2 to −10 MPa for the BC2 stage. The bending of $\sigma_y - \varepsilon_x$ and $\sigma_y - \varepsilon_y$ curves at −2 MPa indicates the effects of changing boundary conditions. The relationship between the normal stress and normal strain is fairly linear at every step. Decreasing strain in the x direction in Fig. 14(a) is due to the Poisson effect influenced by the change of y directional loading.

It is interesting to note the relationships between the normal stresses and shear strains at BC1 and BC2 stages. Fig. 14(b) shows that the normal stress σ_y and shear strain γ_{xy} has a linear response while this behavior cannot be observed in isotropic or orthogonal isotropic materials. The response shown in the graph demonstrates that the S_{61} and S_{62} component in the compliance matrix (Eq. (2)) do play a role in the constitutive relation of fractured rock, and can be effectively estimated by DEM method. However, for the cases concerned in this paper, by comparing the horizontal axes in Figs. 14(a) and (b), it can be noted that the difference in magnitude of the normal and shear strains is very large. Therefore, even though S_{61} and S_{62} can be derived by numerical modeling, their impacts on the overall behavior of fractured rock mass are small for this particular case.

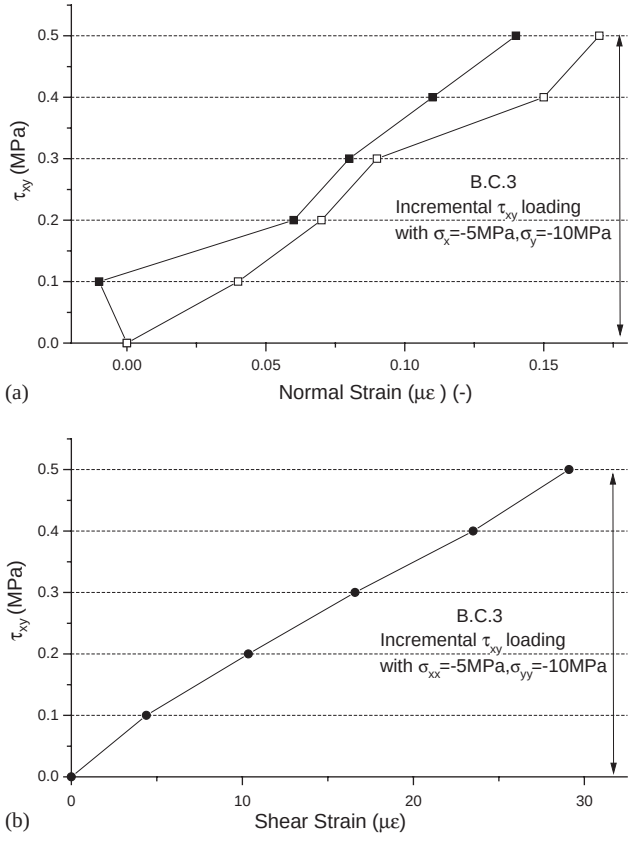

Fig. 15. Stress–strain relation from the sequential numerical experiment (shear stress loading stage, BC3). Model is from DFN3 with size 3 m × 3 m. (a) shear stress–normal strain relationship, (b) shear stress–shear strain relationship. Sign convention is the same as Fig. 14.

The stress–strain relationship at BC3 stage is presented in Fig. 15. The shear stress τ_{xy} is applied sequentially with the increase of 0.1 MPa until 0.5 MPa after the completion of BC1 and BC2 boundary conditions. Fig. 15(a) shows the shear stress versus the normal strains, demonstrating the role of S_{16} and S_{26} components in the compliance matrix. The general behavior shows linear responses of normal strains to the applied shear stresses even if some deviation can be observed. In Fig. 15(b), linearity between the shear stress and shear strain response is clearly illustrated, similar to that between the normal stresses and normal strains shown in Fig. 14(a). Theoretically, because of the assumed symmetry of compliance matrix, the tangent of Figs. 14(b) and 15(a) should be the same. However, some insignificant deviation can be detected, possibly due to numerical approximation errors involved in the averaging process of strains along the sampling lines.

5. Results of scale dependency and tensor characteristics of mechanical properties for fractured rock masses

5.1. Study of the effects of K_s/K_n ratio of fractures on the results of mechanical properties

Fig. 16 presents the variation of the normalized elastic moduli and Poisson's ratios with increasing side lengths of computational models with different K values defined as the ratios of shear stiffness to normal stiffness of fractures in the DFN3 series. The elastic moduli are normalized with the elastic modulus of the intact rock. Results show that the elastic moduli decrease with decreasing K ratio (Fig. 16(a)) and become stable after a certain size, e.g. at a 2–3 m scale. A similar trend can also be observed for Poisson's ratio (Fig. 16(b)). The calculated Poisson's ratio of the fractured rock is smaller than that of the intact rock

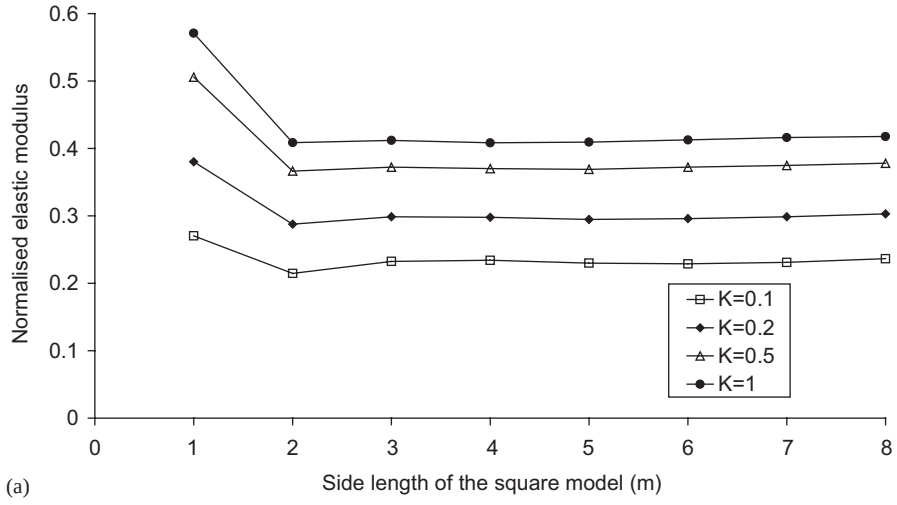

(a)

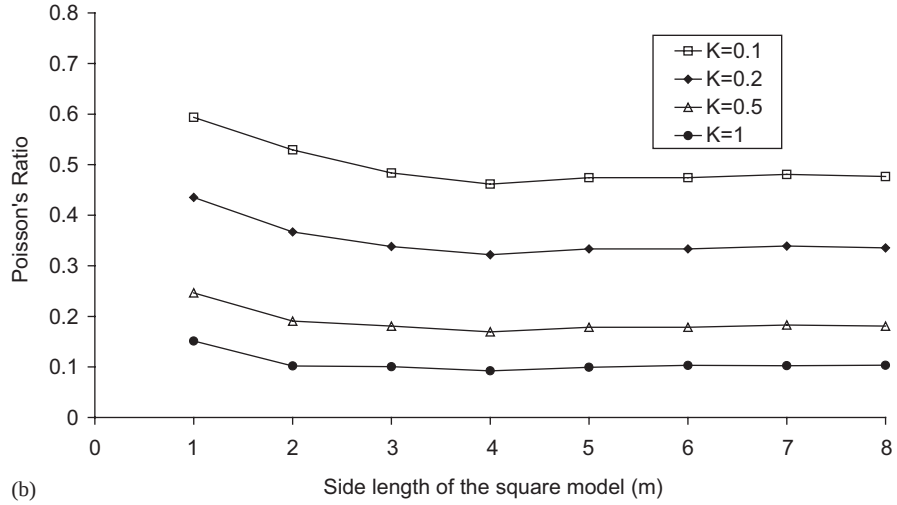

(b)

Fig. 16. Elastic moduli and Poisson's ratio with increasing side lengths of sampling models with different K ratio. DFN3 models from size 1 m × 1 m to 8 m × 8 m were used. (a) Elastic moduli in the x direction and (b) Poisson's ratios (v_{xy}).

(=0.24) with high K ratios (i.e. $K = 0.5$ and 1). This is explained by the fact that the shearing of fracture is constrained due to high shear stiffness of fractures while the normal deformation continues. Conversely, with the low K ratio of 0.1 or 0.2, the Poisson ratio of the fractured rock is higher than that of intact rock due to the low shear stiffness of fractures. For both elastic moduli and Poisson's ratio, the values at 1 m × 1 m scale are the largest of all ten models of different sizes. This is because relatively fewer fractures encompass the DFN 3 model of size 1 m × 1 m. However, this trend may not be general and the property at small scales may become either smaller or larger than that of the models of larger sizes depending on the individual patterns of fracture networks. This potential bias may be more easily encountered if only one single realization is used (as done often in practice) and is the main reason for using multiple stochastic DFN realizations for deriving mechanical properties of fractured rock mass in this study.

5.2. Study of the size effect by multiple realizations of DFN models

Figs. 17 and 18 present the normalized elastic moduli (in the x & y directions) with ten DFN realizations of increasing side lengths from 0.25 to 8 m scales with the K ratio of 1.0 and 0.2, respectively. At the side length less or equal to 1 m, the ranges of the values are notably larger. This scattered data implies that the model at this size cannot be described as statistically homogeneous because one cannot assume a possible stable range of the properties. However, the scattering of the results clearly narrows down with increase of the side lengths, and points to the possible existence of a REV. The mean value of the normalized elastic moduli in x direction is reduced to about 43% of that of the intact rock (Fig. 17(a)) whereas the normalized elastic modulus in y direction is about 50% (Fig. 17(b)). The ratio of E_y to E_x is about 1.2 and this anisotropy is attributable to the effect of orientations of fractures sets. There are more

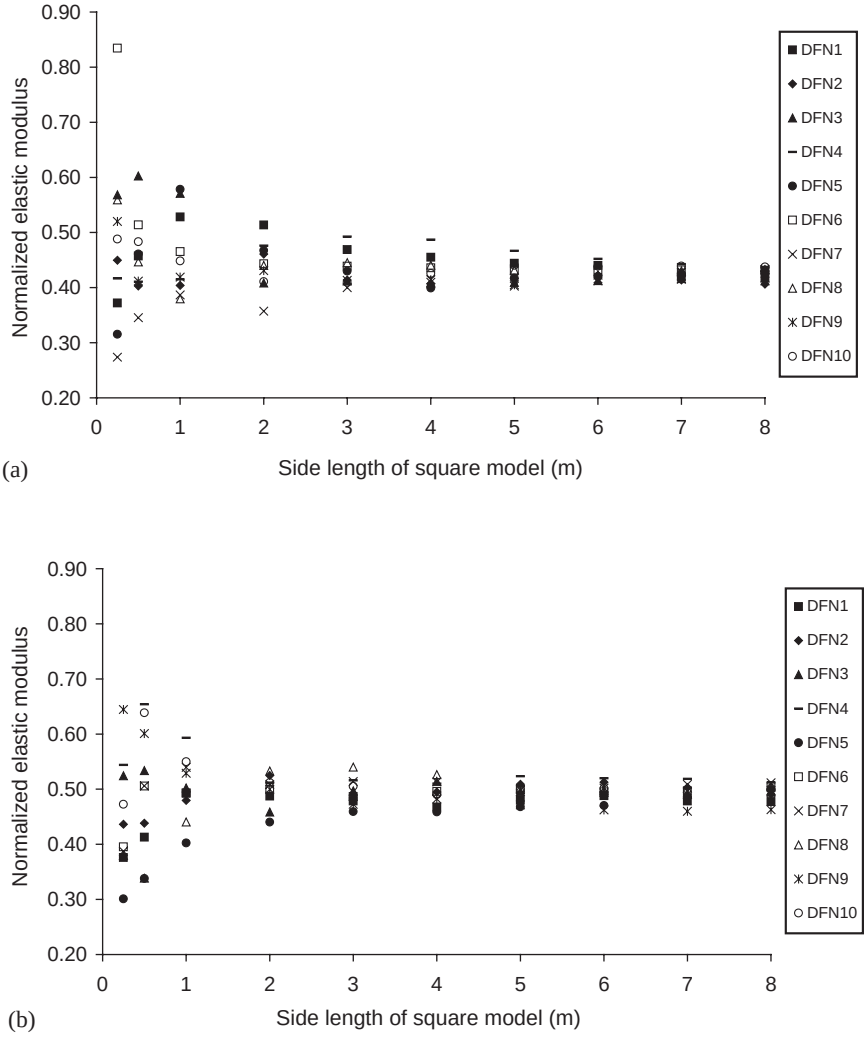

Fig. 17. Variation of elastic modulus with the increase of side lengths of square models ($K = 1.0$). (a) Elastic modulus in the x direction and (b) elastic modulus in the y direction.

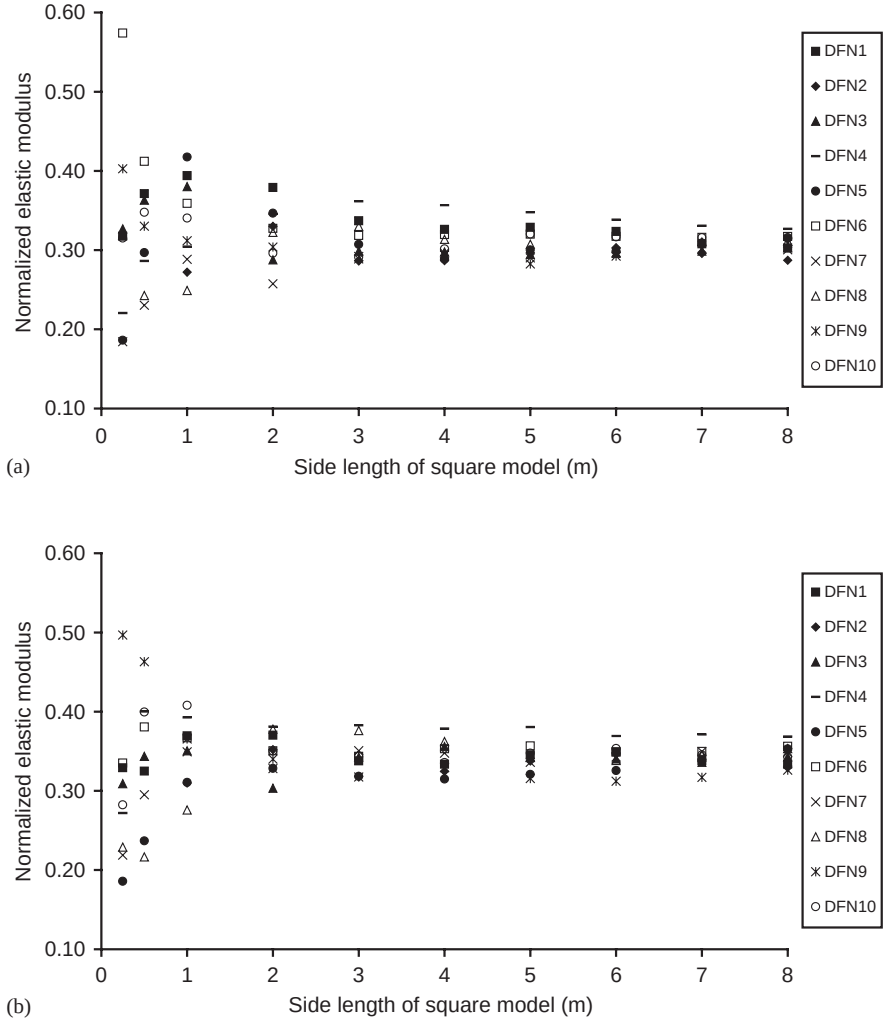

Fig. 18. Variation of elastic modulus with the increase of side lengths of square models ($K = 0.2$). (a) Elastic modulus in the x direction and (b) elastic modulus in the y direction.

fractures in the direction perpendicular to the x axis and this caused the slight anisotropic pattern. Nonetheless, the anisotropy of fractured rock mass for this study is not high. This is explained by highly dispersed fracture orientations by the low Fisher constants and four fracture sets, which made the overall mechanical properties more isotropic. With the K ratio of 0.2 in Fig. 18, the mean values of normalized elastic moduli in x and y directions are about 31% and 34% of that of intact rock, respectively, reduced considerably with the decrease of K ratio.

The results of Poisson's ratio also show a similar pattern and the values converge to about 0.1 and 0.35 for K ratio of 1.0 and 0.2, respectively (Fig. 19). With the K ratio of 1.0, the derived Poisson's ratios are less than half of that of the intact rock ($=0.24$) whereas the derived Poisson's ratio with K ratio of 0.2 is about 50% larger than that of intact rock. Compared to the trend of elastic modulus, Poisson's ratio varies more sensitively with the change of K ratio. The results show that the effect of problem scale, fracture pattern and individual fracture properties can be readily incorporated into the DEM series of numerical experiments.

Figs. 17–19 clearly demonstrate the scale dependency of mechanical properties of fractured rock masses. The properties to be determined have very wide ranges before a certain scale. In both cases, beyond side length of 2–3 m, the scattering range of the properties becomes notably smaller and more constant. Note that mean trace length of fracture is 0.92 m, with 95% of fractures less than 2 m in trace length and 99% of fractures are less than 5 m in trace length, according to the fractal nature of fracture distribution (cf. Eq. (8)). This concentration of smaller fractures is perhaps an important factor for the size of the final REV that cannot be determined by simply checking the stable ranges of these individual properties, but has to be

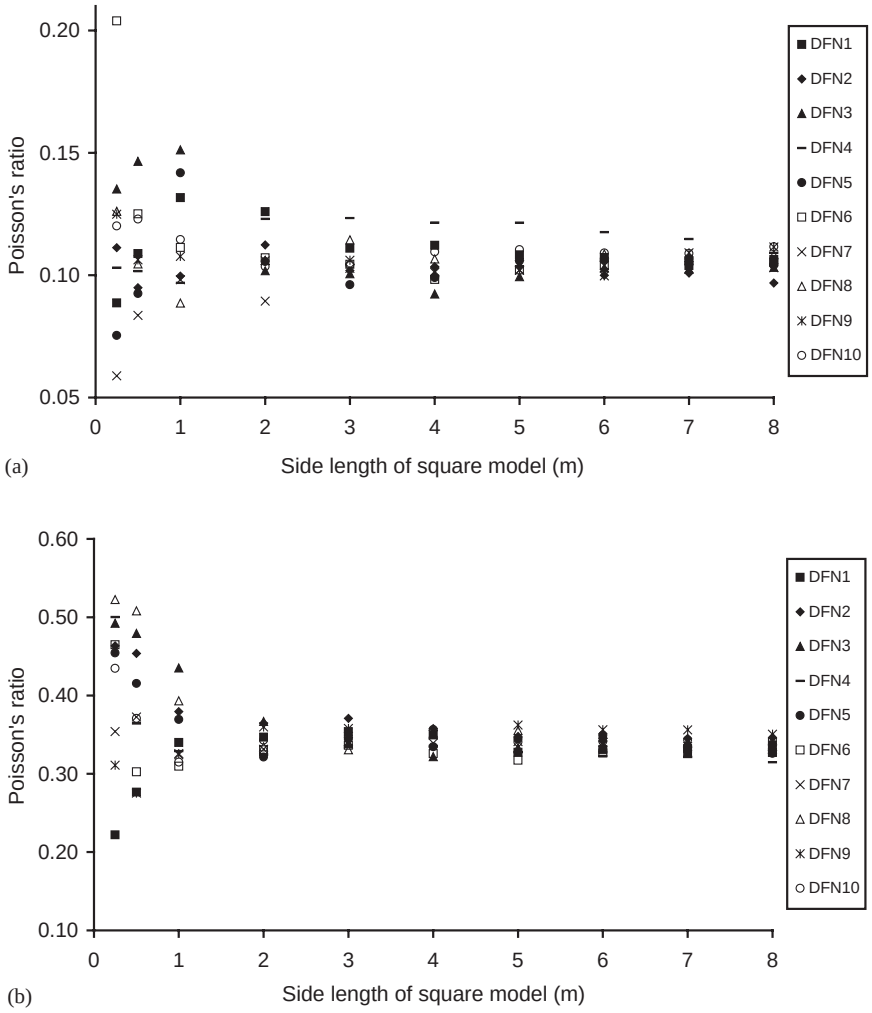

Fig. 19. Variation of Poisson's ratio (v_{xy}) with the increase of side lengths of square models (a) $K = 1.0$ and (b) $K = 0.2$.

determined by whether these properties can be properly approximated in tensor form.

5.3. Fourth-order tensor characteristics of the elastic properties of fractured rock mass, investigated by using numerical experiments in rotated models

It was shown from Eq. (4) that the compliance matrixes in the rotated axes can be constructed using the compliance matrix in the original x–y axes and the matrixes of direction cosines for the rotational operations. In order to evaluate the directional properties of the fractured rock mass under study, the DFN models are rotated in 6 O'clock directions with a 30° interval (0°, 30°, 60°, 90°, 120° and 150°, respectively) to perform similar UDEC simulations in order to calculate the compliance matrixes of the six rotated DFN models. In order to examine whether the calculated elastic properties can be represented by an elastic compliance tensor, an average compliance matrix is calculated by averaging six compliance matrixes from the six rotated DFN models obtained from the numerical experiments, at all different scales. It is important to have a reference axis when matrixes are to be compared or averaged [42] and the original x–y axes were used for this purpose. The average compliance matrix $\bar{S}_{ij}$ is then given by

$$\bar{S}_{ij} = \frac{1}{N}\sum_{r=1}^{N} S^{r}_{pq} q_{pi} q_{qj} \tag{11}$$

where S^{r}_{pq} are the calculated compliance matrixes at rotated p–q axes, and the q_{pi} and q_{qj} are the matrixes of direction cosines of the rotation as defined in Appendix B.

If the average compliance matrix has an acceptable discrepancy with all six compliance matrixes at a certain scale, that scale will determine the size of the REV. Fig. 20 presents the averaged and calculated trace curves of the elastic moduli in the x direction from all the rotated models at different scales for the DFN1 series. The solid curve in the figure for the averaged values is the elastic moduli in the x direction from $\bar{S}_{ij}$ with

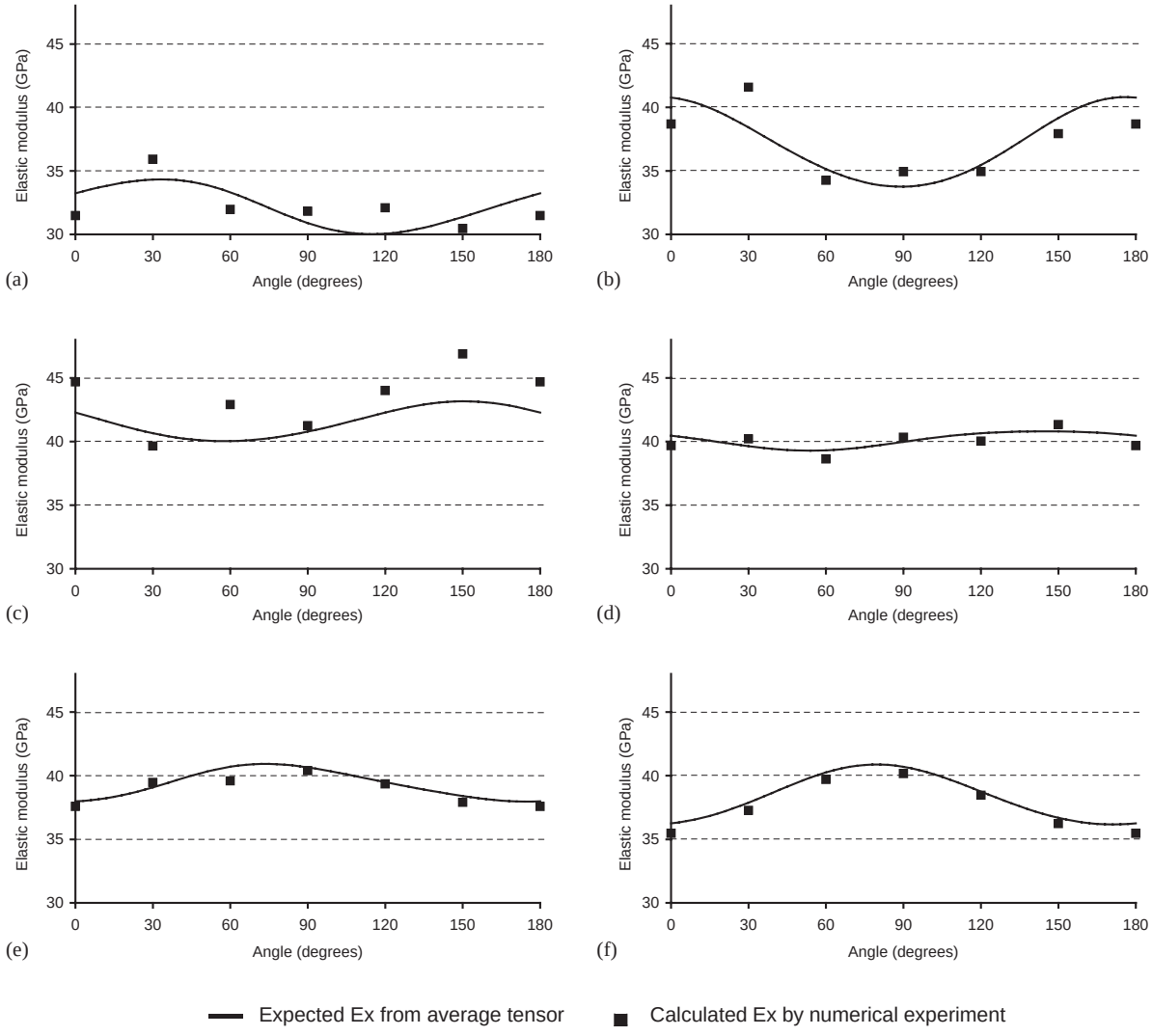

Fig. 20. Comparison between expected and calculated elastic moduli (Ex) in rotated axes. The expected values are calculated from averaged compliance tensor. DFN1 models from side lengths of 0.25 to 7 m were used for the analysis. (a) 0.25 m, (b) 0.5 m, (c) 1 m, (d) 3 m, (e) 5 m and (f) 7 m.

rotations, and the numerical results obtained from the six rotated DFN models at their corresponding rotation directions are plotted as separated symbols.

Fig. 20 shows that the numerical results from the small scales models do not match well with the averaged values. This, in other words, means that the calculated properties do not have a tensor quantity at smaller scales. However, as the size of model increases, the numerical results match increasingly well with the averaged values. At the side length of 5–7 m, the numerical and the averaged trace curves agrees very well, indicating that the property at these sizes can be approximated by a fourth-order tensor. This means that the elastic compliance matrix obtained at the REV scale can be approximated by a fourth-order elastic compliance tensor at a certain degree of accuracy through a proper homogenization (averaging) process.

5.4. Error evaluation in the application of equivalent continuum approach—determination of REV

Determination of REV is a rather subjective task that involves estimating how much resolution is needed for a given purpose. Therefore, it is recommended to associate the REV with the concept of 'acceptable variation'.

A 'coefficient of variation' is defined as the ratio of standard deviation over the mean value of a certain property (say, elastic modulus or Poisson's ratio) obtained from all random DFN models at a given scale. It is used as one of the measures to determine the REV size with given acceptable variation, on the condition that the average value remains constant with increasing scale. Fig. 21(a) presents the coefficient of variations of elastic moduli and Poisson's ratios from the ten realizations as a function of model size. The REV can

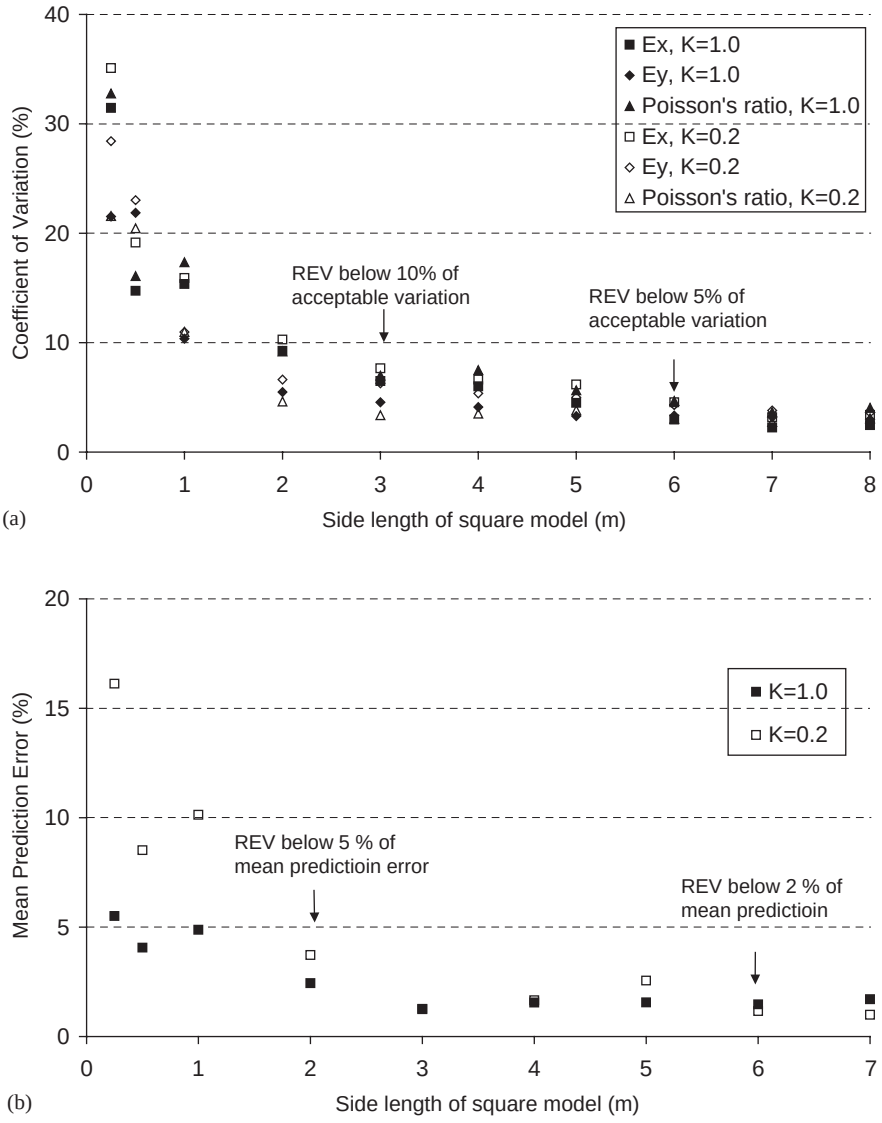

Fig. 21. Error evaluation in the justification of equivalent continuum approach. (a) REV from scale dependency and (b) REV from tensor characteristic evaluation.

be determined according to a chosen 'acceptable variation' from this figure. In this study, the REV can be chosen as 6 m with a 5% of acceptable variation or 3 m scale with a 10% of acceptable variation.

The coefficient of variation is only valid for scalar properties. To evaluate discrepancies between tensors or matrixes, a measure of 'prediction error' of the elastic compliance matrixes is defined to evaluate the errors involved in describing the compliance matrix as fourth-order tensor. The prediction error is intended to represent the discrepancies in the compliance matrixes considering only the effects of the normal strains for simplicity since they are the dominating elements. For two-dimensional cases, this implies that only the first two elements of the compliance matrix need to be considered, and the prediction errors are therefore defined as

$$EPc_i = \frac{1}{N}\frac{\sum_{r=1}^{N}\sum_{j=1}^{2}|s_{ij}^{r} - \bar{s}_{ij}|}{\sum_{j=1}^{2}|\bar{s}_{ij}|} \tag{12}$$

where EPc_i is prediction error of compliance matrix in i direction ($i = x, y$), $\bar{s}_{ij}$ is the average compliance matrix as defined in Eq. (11), s_{ij}^{r} is the compliance matrix from numerical experiments at rotated DFN models and N denotes the number of cases of DFN model rotations ($N = 6$ for this study). Note also that comparison is conducted at the same reference axes.A mean prediction error (μ_{EPc}) can then be defined as the mean values of

Table 5
REV determination based on coefficient of variation and mean prediction error

	Acceptable variation (%)	Mechanical REV
Coefficient of variation (scale dependency)	20	1 m × 1 m
	10	3 m × 3 m
	5	6 m × 6 m
Mean prediction error (tensor quantity evaluation)	10	2 m × 2 m
	5	2 m × 2 m
	2	6 m × 6 m

the two EPc_i, given by

$$\mu_{\mathrm{EPc}} = \tfrac{1}{2}\sum_{i=1}^{2} EPc_i \tag{13}$$

and was used as the collective measure of prediction error for comparisons at different scales, as shown in Fig. 21(b). The size at which the compliance matrix can be approximated by a fourth order compliance tensor depends on a chosen 'acceptable variation' of mean prediction error. From Fig. 17(b), the REV sizes of 2 and 6 m can be decided with acceptable prediction error (acceptable variation) of 5% and 2%, respectively, subject to the needs from practical applications.

In summary, once the acceptable variation for coefficient of variation and mean prediction error are chosen, corresponding REV and the elastic compliance matrix that satisfies both conditions can be selected for an equivalent continuum representation. Table 5 presents the REVs depending upon different acceptable variation (%). Note that the model size that satisfies both 'coefficient of variation' and 'mean prediction error' can be determined as the final REV.

5.5. Final results of elastic compliance tensor

For the test case studied in this paper, an average compliance matrix obtained from ten realizations at 6 m × 6 m scale is presented below for different fracture stiffness ratios (K):

For $K = 1.0$,

$$\begin{pmatrix} S_{11} & S_{12} & S_{13} & S_{16} \\ S_{21} & S_{22} & S_{23} & S_{26} \\ S_{31} & S_{32} & S_{33} & S_{36} \\ S_{61} & S_{62} & S_{63} & S_{66} \end{pmatrix} = \begin{pmatrix} 2.7709 & -0.2933 & -0.2800 & -0.0445 \\ -0.2933 & 2.3934 & -0.2814 & -0.0405 \\ -0.2800 & -0.2814 & 1.1820 & -0.0051 \\ -0.0591 & -0.0653 & -0.0051 & 5.5066 \end{pmatrix} \times E-11 \ (1/\mathrm{Pa}) \tag{14}$$

For $K = 0.2$,

$$\begin{pmatrix} S_{11} & S_{12} & S_{13} & S_{16} \\ S_{21} & S_{22} & S_{23} & S_{26} \\ S_{31} & S_{32} & S_{33} & S_{36} \\ S_{61} & S_{62} & S_{63} & S_{66} \end{pmatrix} = \begin{pmatrix} 3.8389 & -1.3073 & -0.2808 & -0.2039 \\ -1.3097 & 3.4556 & -0.2812 & 0.1151 \\ -0.2808 & -0.2812 & 1.1820 & -0.0012 \\ -0.2336 & 0.1018 & 0.0012 & 10.683 \end{pmatrix} \times E-11(1/\mathrm{Pa}) \tag{15}$$

Note that the compliance matrix is almost symmetric, diagonally dominant and with almost zero contributions by the shear stresses to the out-of-plane normal strain ε_z and the out-of-plane normal stress σ_z to the in-plane shear strain γ_{xy}, represented by very small values of elements S_{36} and S_{63}, respectively. Because the symmetry assumption of $S_{31} = S_{13}$ and $S_{32} = S_{23}$ was initially used for determination of the components, the symmetry appears in Eqs. (14) and (15) is not related to the accuracy of numerical experiments. However, the near symmetrical feature of the other components, namely S_{12} and S_{21}, S_{16} and S_{61}, and S_{26} and S_{62}, are determined by the numerical solutions. This is in part due to the averaging process from ten realizations where the non-symmetry contributions from different realizations are somehow compensated. However, the symmetry deviation in each individual realization was also below 5% for the diagonal components. The accuracy of the calculated results can be further evaluated by comparing S_{13}, S_{23} and S_{36} using Fig. 8. S_{13} and S_{23} are calculated as 0.28370E−11 (/Pa) with the Poisson ratio of 0.24 and elastic modulus of 84.6 GPa of the intact rock (Table. 3). The difference between the numerically calculated value (0.28E−11) and the theoretical solution obtained by Fig. 8 is small (less than 2%). Furthermore, S_{36} is very close to zero, which is also similar to the assumed behavior shown in Fig. 8. This result supports the numerical experiment approach presented in this paper.

With the determined nearly symmetric compliance matrix as shown in Eq. (14) or Eq. (15), it is easy to derive a symmetric compliance tensor $[\mathbf{S}_{ij}]$ by a simple averaging operation as

$$(\mathbf{S}_{ij}) = \tfrac{1}{2}[(S_{ij}) + (S_{ij})^{\mathrm{T}}] \tag{16}$$

where $(S_{ij})^{\mathrm{T}}$ is the transpose of the compliance matrix (S_{ij}) that is supported by a REV of 6 m in linear scale and can be used as the elastic properties for continuum analysis.

6. Conclusion and discussion

This paper presented a systematic description of a numerical approach for deriving equivalent elastic properties of fractured rock masses with irregular and randomly distributed fracture systems, including the REV concept, tensor representation of mechanical properties and their subjective determination regarding discrepancies caused by random realizations of fracture systems. The main conclusions are summarized as follows:

(1) An approach using numerical experiments is successfully developed for the determination of equivalent mechanical properties of fractured rock masses using the distinct element method based on the geometry of DFNs. The elastic compliance tensor is calculated using multiple realizations of stochastic fracture networks based on generalized Hooke's law.

The strength of the numerical approach over other empirical or analytical methods is that the mechanical properties of fractured rock mass with very irregular fracture system geometry can be directly determined and that complex constitutive models of fractures can be incorporated. Using this approach, we can investigate the effect of different factors in the determination of overall mechanical properties by sensitivity analysis, and using Monte Carlo simulation approach to conduct probabilistic estimation of rock properties.

It should be noted that numerical experiments are highly dependent on the knowledge of the fracture geometry and fracture constitutive relations. The constitutive model for the fractures in this analysis is a constant elastic stiffness model, describing a linear relationship between the stress and displacement in fractures. A more realistic fracture constitutive model with hyperbolic relations can be used by the developed methodology without any undue difficulty and will give a more realistic rock mass behavior, leading to a stress-dependent compliance matrix. Further investigations with the inclusion of failure and dilation of fracture can be conducted on the strength of rock mass for more general characterization of fractured rock masses.

(2) Scale dependency of mechanical properties of the rock mass under study are thoroughly investigated by the numerical experiments on multiple series of models with varying sizes. The results in this paper demonstrate the existence of REV for the fractured rock mass with the given fracture data, achieved by the converging ranges of mechanical properties with the increasing side lengths of square DFN models. Due to the stochastic nature of DFN models, the properties at REV have ranges of values instead of single values.

Many factors will have an influence on the REV, namely fracture properties, constitutive relations, distributions of trace length, orientation and locations of fractures. When the statistics of fractures are homogeneous, it is probable that REV may exist at certain scales, as demonstrated by this study. However, existence of REV for fractured rock masses is site specific, especially regarding the effects of fracture statistics and deformation characteristics.

(3) It is demonstrated that the compliance tensor in rotated axes can be predicted from the one in original axes with an acceptable accuracy, as long as it is estimated at support volumes nor less than an existing REV. This implies that fractured rock masses of equivalent statistical homogeneity of fracture systems can be represented as a homogeneous continuum above a certain scale.

This technique is achieved by extending the approach of the second-order permeability tensor to the fourth-order elastic compliance tensor for fractured rock mass. The method presented in this paper justifies the use of continuum mechanics principle for the fractured rock mass under the geological conditions defined in this study.

(4) In order to evaluate the two criteria for the appropriateness of equivalent continuum approach, two measures has been suggested: 'coefficient of variation' to be used to evaluate the variation from the multiple realization of stochastic DFNs and 'mean prediction error' to be used for the evaluation of error involved in the prediction of compliance tensor in rotated axes.

These measures give a tool for the quantitative evaluation of the uncertainties related to the application of the equivalent continuum approach in terms of scale dependency and random variation of fracture systems.

Acknowledgements

The authors acknowledge the financial support of the Swedish Nuclear Inspectorate (SKI) through the DECOVALEX III project and the European Commission through the BENCHPAR project (FIKW-CT-2000-00066) for the work presented in this paper. The authors also thank Professor O. Stephansson of the Royal Institute of Technology (KTH), Sweden and Professor J. A. Hudson of Imperial College, UK, for their encouraging comments during the research work and for reviewing the paper. Ms Sandra Brunsberg of the Royal Institute of Technology is acknowledged for checking the English of the manuscript.

Appendix A. Explicit expression of compliance matrix for constitutive relation of anisotropic media

Eq. (2) can be explicitly expressed as follows by assigning a physical meaning in all components [35]:

$$\begin{pmatrix} \varepsilon_x \\ \varepsilon_y \\ \varepsilon_z \\ \gamma_{yz} \\ \gamma_{xz} \\ \gamma_{xy} \end{pmatrix} = \begin{pmatrix} \frac{1}{E_x} & -\frac{\nu_{yx}}{E_y} & -\frac{\nu_{zx}}{E_z} & \frac{\eta_{x,yz}}{G_{yz}} & \frac{\eta_{x,xz}}{G_{xz}} & \frac{\eta_{x,xy}}{G_{xy}} \\ -\frac{\nu_{xy}}{E_x} & \frac{1}{E_y} & -\frac{\nu_{zy}}{E_z} & \frac{\eta_{y,yz}}{G_{yz}} & \frac{\eta_{y,xz}}{G_{xz}} & \frac{\eta_{y,xy}}{G_{xy}} \\ -\frac{\nu_{xz}}{E_x} & -\frac{\nu_{yz}}{E_y} & \frac{1}{E_z} & \frac{\eta_{z,yz}}{G_{yz}} & \frac{\eta_{z,xz}}{G_{xz}} & \frac{\eta_{z,xy}}{G_{xy}} \\ \frac{\eta_{yz,x}}{E_x} & \frac{\eta_{yz,y}}{E_y} & \frac{\eta_{yz,z}}{E_z} & \frac{1}{G_{yz}} & \frac{\mu_{yz,xz}}{G_{xz}} & \frac{\mu_{yz,xy}}{G_{xy}} \\ \frac{\eta_{xz,x}}{E_x} & \frac{\eta_{xz,y}}{E_y} & \frac{\eta_{xz,z}}{E_z} & \frac{\mu_{xz,yz}}{G_{yz}} & \frac{1}{G_{xz}} & \frac{\mu_{xz,xy}}{G_{xy}} \\ \frac{\eta_{xy,x}}{E_x} & \frac{\eta_{xy,y}}{E_y} & \frac{\eta_{xy,z}}{E_z} & \frac{\mu_{xy,yz}}{G_{yz}} & \frac{\mu_{xy,xz}}{G_{xz}} & \frac{1}{G_{xy}} \end{pmatrix} \begin{pmatrix} \sigma_x \\ \sigma_y \\ \sigma_z \\ \tau_{yz} \\ \tau_{xz} \\ \tau_{xy} \end{pmatrix} \tag{A.1}$$

where E_x, E_y, E_z are the elastic moduli in the x, y and z directions; G_{yz}, G_{xz}, G_{xy} are the shear moduli in yz, xz and xy planes; $\nu_{xy}, \nu_{yx}, \nu_{zx}, \nu_{xz}, \nu_{yz}, \nu_{zy}$ are Poisson's ratios (the property ν_{ij} determines the ratio of strain in the j direction to the strain in the i direction due to a stress acting in the i direction); $\mu_{yz,xz}, \mu_{yz,xy}, \mu_{xz,yz}, \mu_{xz,xy}, \mu_{xy,yz}, \mu_{xy,xz}$ are the coefficients of Chentsov. The symbol $\mu_{ij,kl}$ characterizes the shear in the plane parallel to the one defined by indices ij that induces the tangential stress in the plane parallel to the one defined by indices kl. $\eta_{x,yz}, \eta_{x,xz}, \eta_{x,xy}, \eta_{y,yz}, \eta_{y,xz}, \eta_{y,xy}, \eta_{z,yz}, \eta_{z,xz}, \eta_{z,xy}$ are the coefficients of mutual influence of the first kind. $\eta_{k,ij}$ characterizes the stretching in the k direction induced by the shear stress acting within a plane parallel to the one defined by indices ij; $\eta_{yz,x}, \eta_{yz,y}, \eta_{yz,z}, \eta_{xz,x}, \eta_{xz,y}, \eta_{xz,z}, \eta_{xy,x}, \eta_{xy,y}, \eta_{xy,z}$ are the coefficients of mutual influence of the second kind; $\eta_{ij,k}$ characterizes a shear in the plane defined by indices ij under the influence of a normal stress acting in the k direction.

From the symmetry of compliance matrix, following relation is valid:

$$\frac{\nu_{ij}}{E_i} = \frac{\nu_{ji}}{E_j}, \quad \frac{\mu_{ik,jk}}{G_{jk}} = \frac{\mu_{jk,ik}}{G_{ik}}, \quad \frac{\eta_{ij,k}}{E_k} = \frac{\eta_{k,ij}}{G_{ij}} \tag{A.2}$$

Appendix B. Expression of direction cosine in (6×6) matrix form [35]

Tables 6 and 7 present the component of transformation matrix presented in Eqs. (3) and (4).

Table 6
Symbols for the direction cosines in rectangular x-,y-,z-axis and x'-,y'-,z'-axis

	x	y	z
x'	α_1	β_1	γ_1
y'	α_2	β_2	γ_2
z'	α_3	β_3	γ_3

Table 7
The q_{ij} matrix components

	1	2	3	4	5	6
1	α_1^2	α_2^2	α_3^2	$2\alpha_2\alpha_3$	$2\alpha_3\alpha_1$	$2\alpha_1\alpha_2$
2	β_1^2	β_2^2	β_3^2	$2\beta_2\beta_3$	$2\beta_3\beta_1$	$2\beta_1\beta_2$
3	γ_1^2	γ_2^2	γ_3^2	$2\gamma_2\gamma_3$	$2\gamma_3\gamma_1$	$2\gamma_1\gamma_2$
4	$\beta_1\gamma_1$	$\beta_2\gamma_2$	$\beta_3\gamma_3$	$\beta_2\gamma_3 + \beta_3\gamma_2$	$\beta_1\gamma_3 + \beta_3\gamma_1$	$\beta_1\gamma_2 + \beta_2\gamma_1$
5	$\gamma_1\alpha_1$	$\gamma_2\alpha_2$	$\gamma_3\alpha_3$	$\gamma_2\alpha_3 + \gamma_3\alpha_2$	$\gamma_1\alpha_3 + \gamma_3\alpha_1$	$\gamma_1\alpha_2 + \gamma_2\alpha_1$
6	$\alpha_1\beta_1$	$\alpha_2\beta_2$	$\alpha_3\beta_3$	$\alpha_2\beta_3 + \alpha_3\beta_2$	$\alpha_1\beta_3 + \alpha_3\beta_1$	$\alpha_1\beta_2 + \alpha_2\beta_1$

References

[1] Sitharam TG, Sridevi J, Shimizu N. Practical equivalent continuum characterization of jointed rock masses. Int J Rock Mech Min Sci 2001;38(3):437–48.

[2] Long JCS, Remer JS, Wilson CR, Witherspoon PA. Porous media equivalents for networks of discontinuous fractures. Water Resour Res 1982;18(3):645–58.

[3] Hart RD. An introduction to distinct element modeling for rock engineering. In: Hudson JA, editor. Comprehensive rock engineering, vol. 2. Oxford: Pergamon Press, 1993. p. 245–61.

[4] Jing L. Formulations of discontinuous deformation analysis for block systems. Eng Geology 1998;49:371–81.

[5] Bieniawski ZT. Determining rock mass deformability: experience from case histories. Int J Rock Mech Min Sci Geomech Abstr 1978;15:237–47.

[6] Barton N. Some new Q-value correlations to assist in site characterization and tunnel design. Int J Rock Mech Min Sci 2002;39(2):185–216.

[7] Hoek E, Brown ET. Practical estimates of rock mass strength. Int J Rock Mech Min Sci Geomech Abstr 1997;34(8):1165–86.

[8] Palmström A. Characterizing rock masses by the RMi for use in practical rock engineering, Part 2: Some practical applications of the rock mass index (RMi). Tunnelling Underground Space Technol 1996;11(3):287–303.

[9] Ramamurthy T. Strength and modulus responses of anisotropic rocks. In: Hudson JA, editor. Comprehensive rock engineering, vol. 1. Oxford: Pergamon Press, 1993. p. 313–29.
[10] Marinos P, Hoek E. GSI: a geologically friendly tool for rock mass strength estimation. GeoEng2000; An International Conference on Geotechnical and Geological Engineering, Melbourne, vol. 2. Pennsylvania: Technomic, 2000.
[11] Holland KL, Lorig LJ. Numerical examination of empirical rock-mass classification systems. Int J Rock Mech Min Sci Geomech Abstr 1997;34(3/4):127.
[12] Salamon MDG. Elastic moduli of a stratified rock mass. Int J Rock Mech Min Sci GeoMech Abstr 1968;5:519–27.
[13] Singh B. Continuum characterization of jointed rock masses. Int J Rock Mech Min Sci Geomech Abstr 1973;10:311–35.
[14] Gerrard CM. Elastic models of rock masses having one, two and three sets of joints. Int J Rock Mech Min Sci Geomech Abstr 1982;19:15–23.
[15] Stephansson O. The Näsliden project-rock mass investigations. In: Stephansson O, Jone MJ, editors. Application of rock mechanics to cut and fill mining. London: IMM, 1981. p. 145–61.
[16] Fossum AF. Effective elastic properties for a randomly jointed rock mass. Int J Rock Mech Min Sci Geomech Abstr 1985;22(6):467–70.
[17] Amadei B,Goodman RE. A3-D constitutive relation for fractured rock masses. In: Selvadurai APS, editor. Proceedings of the International Symposium on the Mechanical Behavior of Structured Media, Ottawa, Part B, 1981. p. 249–68.
[18] Hu KX, Huang Y. Estimation of the elastic properties of fractured rock masses. Int J Rock Mech Min Sci Geomech Abstr 1993;30(4):381–94.
[19] Oda M. Fabric tensor for discontinuous geological materials. Soils Fdns 1982;22(4):96–108.
[20] Oda M. Similarity rule of crack geometry in statistically homogeneous rock masses. Mech Mater 1984;3:119–29.
[21] Kulatilake PHSW, Wang S, Stephansson O. Effects of finite-size joints on the deformability of jointed rock in three dimensions. Int J Rock Mech Min Sci 1993;30(5):479–501.
[22] Pouya A, Ghoreychi M. Determination of rock mass strength properties by homogenization. Int J Numer Anal Meth Geomech 2001;25:1285–303.
[23] Stietel A, Millard A, Treille E, Vuillod E, Thoraval A, Ababon R. Continuum Representation of coupled hydromechanic processes of fractured media: homogenization and parameter identification. In: Stephansson O et al., editors. Coupled thermo-hydro-mechanical processes of fractured media: developments in geotechnical engineering. Amsterdam: Elsevier Science, 1996. p. 135–64.
[24] Ivars DM, Min KB, Jing L. Homogenization of mechanical properties of fractured rocks by DEM modeling. Proceedings of the Second Asian Rock Mechanics Symposium, 2001, Beijing, China. Rotterdam, Balkema. p. 311–4.
[25] Min KB, Ivars DM, Jing L, Numerical derivation of the equivalent hydro-mechanical properties of fractured rock masses using Distinct Element Method, DC Rocks 2001 38th US Symposium on Rock Mechanics, Washington, DC, 2001. p. 1469–76.
[26] La Pointe PL, Wallmann PC, Follin S. Continuum modeling of fractured rock masses: is it useful? In: Barla G, editor. Eurock 96. Rotterdam: Balkema, 1996. p. 343–50.
[27] Aydan Ö, Jeong GC, Seiki T, Akagi T. A comparative study on various approaches to model discontinuous rock mass as equivalent continuum. In: Rossmanith HP, editor. Mechanics of jointed and faulted rock, 1995. p. 569–74.
[28] Bear J. Dynamics of fluids in porous media. New York: Dover, 1972. p. 764.
[29] Long JCS, Witherspoon PA. The relationship of the degree of interconnection to permeability in fracture networks. J Geophys Res 1985;90(B4):3087–98.
[30] Pariseau WG. Non-representativ evolume element modeling of equivalent jointed rock mass properties. In: Rossmanith HP, editor. Mechanics of jointed and faulted rock, 1995. p. 563–8.
[31] Min KB. Determination of equivalent hydraulic, mechanical properties of fractured rock masses using the distinct element method. Licentiate Thesis, Royal Institute of Technology, Stockholm, Sweden, 2002.
[32] Itasca Consulting Group, Inc. UDEC user's guide, Minnesota, 2000.
[33] DECOVALEX III secretariat, TASK 3, BMT2 protocol, version 6.0, Stockholm, 2000, unpublished report.
[34] Ting TCT. Anisotropic elasticity—theory, applications. Oxford: Oxford University Press, 1996. p. 570.
[35] Lekhnitskii SG. Theory of elasticity of an anisotropic elastic body. San Francisco: Holden Day Inc., 1963. p. 404.
[36] Wei ZQ, Hudson JA. The influence of joints on rock modulus. In: Tan ZY, editor. Proceeding of the International Symposium on Engineering in Complex Formations, Peking. Moscow: Science Press, 1986. p. 54–62.
[37] Wei ZQ. A fundamental study of the deformability of rock masses. Ph.D. thesis, Imperial College, University of London, 1988.
[38] Priest SD. Discontinuity analysis for rock engineering. London: Chapman & Hall, 1993. p. 473.
[39] Jang HI, Chang KM, Lee CI. Groundwater flow analysis of discontinuous rock mass with probabilistic approach. J Korean Soc Rock Mech 1996;6:30–8 [in Korean].
[40] Min KB, Jing L, Stephansson O. Determination of the permeability tensor of fractured rock masses based on stochastic REV approach. ISRM Regional Symposium, Third Korea–Japan Joint Symposium on Rock Engineering, vol. 1, Seoul, Korea, 2002. p. 289–96.
[41] Nirex. Evaluation of heterogeneity, scaling of fractures in the Borrowdale volcanic group in the Sellafield area. Nirex Report SA/97/028, 1997.
[42] Hudson JA, Harrison JP. Engineering rock mechanics, Amsterdam: Pergamon, 1997. p. 444.